Escort Tug Performance Prediction: A CFD Method

by

Brendan Smoker
B. Eng, University of Victoria, 2009

A Dissertation Submitted in Partial Fulfillment
of the Requirements for the Degree of

MASTER OF APPLIED SCIENCE

in the Department of Mechanical Engineering

Supervisory Committee

Escort Tug Performance Prediction: A CFD Method

by

Brendan Smoker
B. Eng, University of Victoria, 2009

Supervisory Committee

Dr. Peter Oshkai, (Department of Mechanical Engineering)
Supervisor

Dr. Brad Buckham, (Department of Mechanical Engineering)
Departmental Member

Dr. Rustom Bhiladvala, (Department of Mechanical Engineering)
Departmental Member

Dr. Ian Walker, (Department of Geography)
Outside Member

Abstract

As the demand for energy continues to increase around the world, more vessels used in the transport of energy, such as Liquid Natural Gas (LNG) and crude oil tankers are being built to transport energy to market overseas. The escort tug has been developed in order to assist in the safe transit of such vessels in confined waterways. Designed to apply emergency braking and steering forces to the stern of a tanker while underway, an escort tug features a hull shape that generates large hydrodynamic lift and drag forces when operating at high angles of attack, this is known as indirect mode. This escorting mode is highly effective at speeds 8 knots and above, often generating towline forces well in excess of bollard pull.

Escort performance prediction is a vital aspect of the design of escort tugs. It is important to know *a priori* if a design will meet the necessary performance criteria. In the past, performance predictions have relied heavily on model testing and empirical methods. With the recent emergence of Computational Fluid Dynamics (CFD) as a commercially viable design tool for naval architects, extensive escort performance predictions can now be carried out more accurately in less time and at less cost than was previously possible.

This thesis describes the methodology of a CFD based escort performance prediction method that is accurate and cost effective.

Table of Contents

List of Tables

List of Figures

Acknowledgments

I wish to thank Robert Allan Ltd., the Natural Sciences and Engineering Research Council (NSERC) and the University of Victoria for partnering to make this project possible. I am grateful to the many Robert Allan Ltd. employees who assisted me in my research while I spent time at their firm. I especially wish to acknowledge Bart Stockdill, Vince den Hertog, Oscar Lisagor, and Todd Barber, at Robert Allan Ltd. for spending the time to explain all I could wish to know about Naval Architecture and the design and operation of Escort Tugs.

I also want to thank my supervisor, Dr. Peter Oshkai, who patiently supported me in learning the science of CFD and who also guided me through the graduate process at UVic.

Finally, I owe my thanks to my family, friends and wife, Andrea, who supported me with their encouragement and patience.

Dedication

To Andrea

Abbreviations

LNG	Liquid Natural Gas
CFD	Computational Fluid Dynamics
ASD	Azimuthing Stern Drive
SIMPLE	Semi-Implicit Method for Pressure-Linked Equations
IMD	Institute for Marine Dynamics
DFBI	Dynamic Fluid Body Interaction
VOF	Volume of Fluid
CG	Center of Gravity
CLR	Center of Lateral Resistance
LCG	Longitudinal Distance to Center of Gravity
TCG	Transverse Distance to Center of Gravity
VCG	Vertical Distance to Center of Gravity
LZD	Longitudinal Distance to Center of Z-Drive Thrust
TZD	Transverse Distance to Center of Z-Drive Thrust
VZD	Vertical Distance to Center of Z-Drive Thrust
LTS	Longitudinal Distance to Towing Staple
TTS	Transverse Distance to Towing Staple
VTS	Vertical Distance to Towing Staple

Chapter 1

Introduction

With the ever increasing frequency of perceived high risk marine traffic, such as Liquid Natural Gas (LNG) and crude oil tankers, it has become necessary to take further steps to ensure transit safety through the introduction of the escort tugboat. An escort tug is unique in that it is designed specifically for the task of applying steering and braking forces to the escorted vessel at full transit speeds. Contrary to a traditional tug which primarily relies on direct force methods, escort tugs take advantage of an indirect mode. This indirect mode utilizes hydrodynamic pressure effects experienced by the skeg, a large vertical fin extending down from the hull, and hull of the escort tug to create significant braking and steering forces at speeds greater than 8 knots. The design of an escort tug must be such that it can counter the turning effects of a malfunctioning rudder fixed hard-over to one side. Due to the stringent requirements of an escort class tug of high manoeuvrability and thrust, a limited number of tugs are classified for escort duty.

Performance prediction is a vital aspect of the design process of escort tugs as it is important to know *a priori* if a design will meet the given performance criteria. Significant research has been done on vessel resistance and on the scaling effects of model based experimental tests. In the past, design performance strategies relied heavily on extensive model tests; however, the emergence of Computational Fluid Dynamics (CFD) has provided designers with a tool to facilitate more frequent and extensive pre-construction vessel performance studies than previously possible. While model basin tests still exist as the definitive method for quantifying a vessel's performance, their role has also begun to shift towards that of CFD validation. With the increased usability and

accessibility of CFD, the potential exists to develop new and improved methods for calculating the performance of escort tugs while they are still in the design phase. The purpose of this thesis is to outline a method using CFD to predict the steering and braking forces of an escort tug.

Current methods do exist to convert hydrodynamic escort tug body forces into towline and thrust forces; however, these methods are developed and used for commercial escort performance predictions and are not available in the public domain. Additionally, the existing methods estimate the hydrodynamic forces on the escort tug using the lateral hull and skeg wetted area. The method proposed in this thesis uses the calculated hydrodynamic forces determined in CFD which includes free surface and flow separation effects as well as the ship heave (vertical translation) and roll angle (longitudinal rotation). In demonstrating that such an analysis is accurate and practical, the standard of escort force prediction can be raised to one that utilizes specific ship geometry rather than estimated lift and drag coefficients derived from first principles.

1.1 Escort Tugs

An example of an escort tug is shown in Figure 1.1. Four key aspects of an escort tug are the: towing staple, escort winch, skeg and method of thrust, in this case azimuthing stern drives (Z-drives).

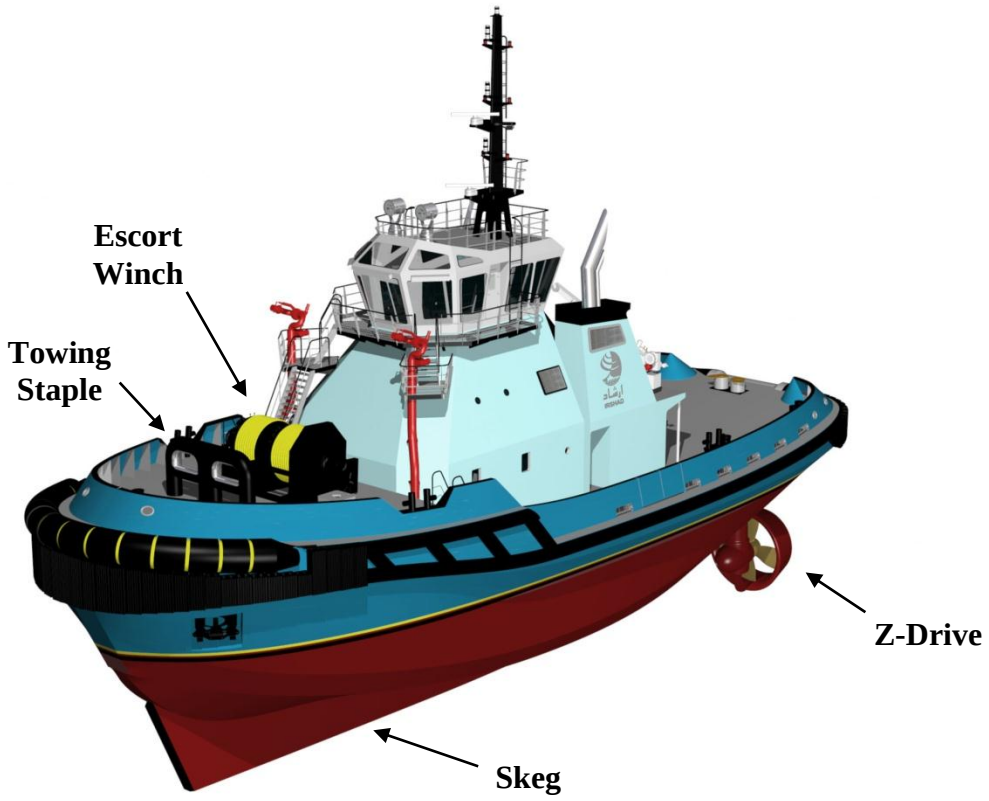

Figure 1.1: *RAstar 3500* ASD Escort Tug *Irshad* [Robert Allan Ltd.]

In general there are two types escort tugs in use: azimuth stern drive (ASD) tugs and tractor tugs. ASD tugs are characterized by their longer, shallow skeg and dual Z-drives at the stern. Z-drives are a method of propulsion that features a propeller attached to a drive leg extending down from the hull. The leg allows the drive to rotate 360°, providing increased manoeuvrability over conventional fixed shaft and propeller tugs. Tractor tugs have their drives positioned near the bow with a shorter, deeper skeg at the stern. An

ASD tug escorts bow first while a tractor tug escorts stern first. Therefore, the skeg in both cases is always facing the escorted ship.

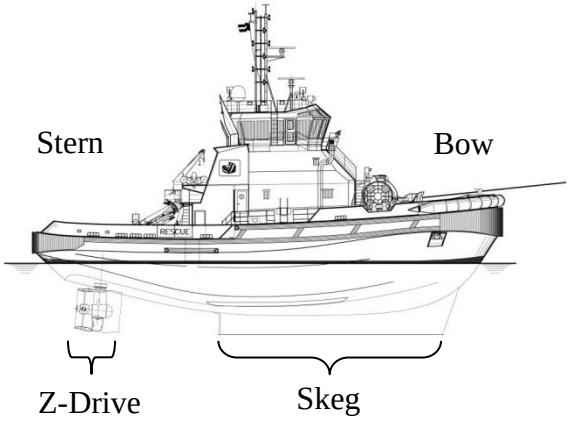

Figure 1.2: ASD Escort Tug[1]

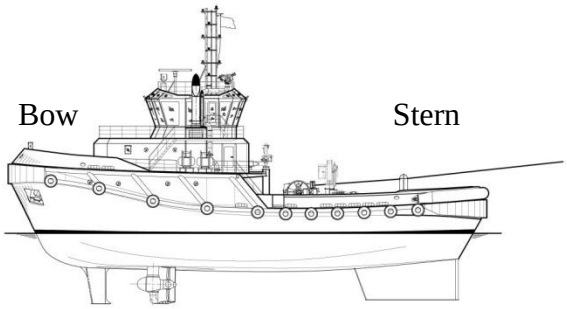

Figure 1.3: Tractor Escort Tug

The steering and braking forces created by the escort tug are applied by way of a towline going from the stern of the escorted vessel to the staple-winch arrangement on the tug. The towline force applied by the tug to the vessel can be separated into two components: braking force, caused by tug drag in the direction of motion of the escorted vessel, and steering force, caused by hull hydrodynamic lift. The braking and steering force component are also augmented by the forces generated by the Z-drives. The two primary categories of escort methods available to a tug operator are defined as the direct methods and indirect methods. An ASD tug is shown escorting in indirect mode in Figure 1.4.

[1] Escort tug drawings provided courtesy of Robert Allan Ltd.

Figure 1.4: Escort Tug Foss America Escorting in Indirect Mode [Robert Allan Ltd.]

When considering the tug center of gravity as a reference point, the primary forces acting on an escort tug in indirect mode are:

- Towline tension;
- Net thrust force;
- Hydrodynamic Lift Force;
- Hydrodynamic Drag Force; and,
- Hydrodynamic Yawing Moment.

The escort tug applies force to the escorted ship through the towline. The longitudinal component of the towline force with respect to the escorted ship motion is referred to as the escort braking force and the transverse component is referred to as the escort steering force. The maximum sustainable braking and steering forces generated by the tug determine its escort performance. The pertinent escort forces are shown in Figure 1.5.

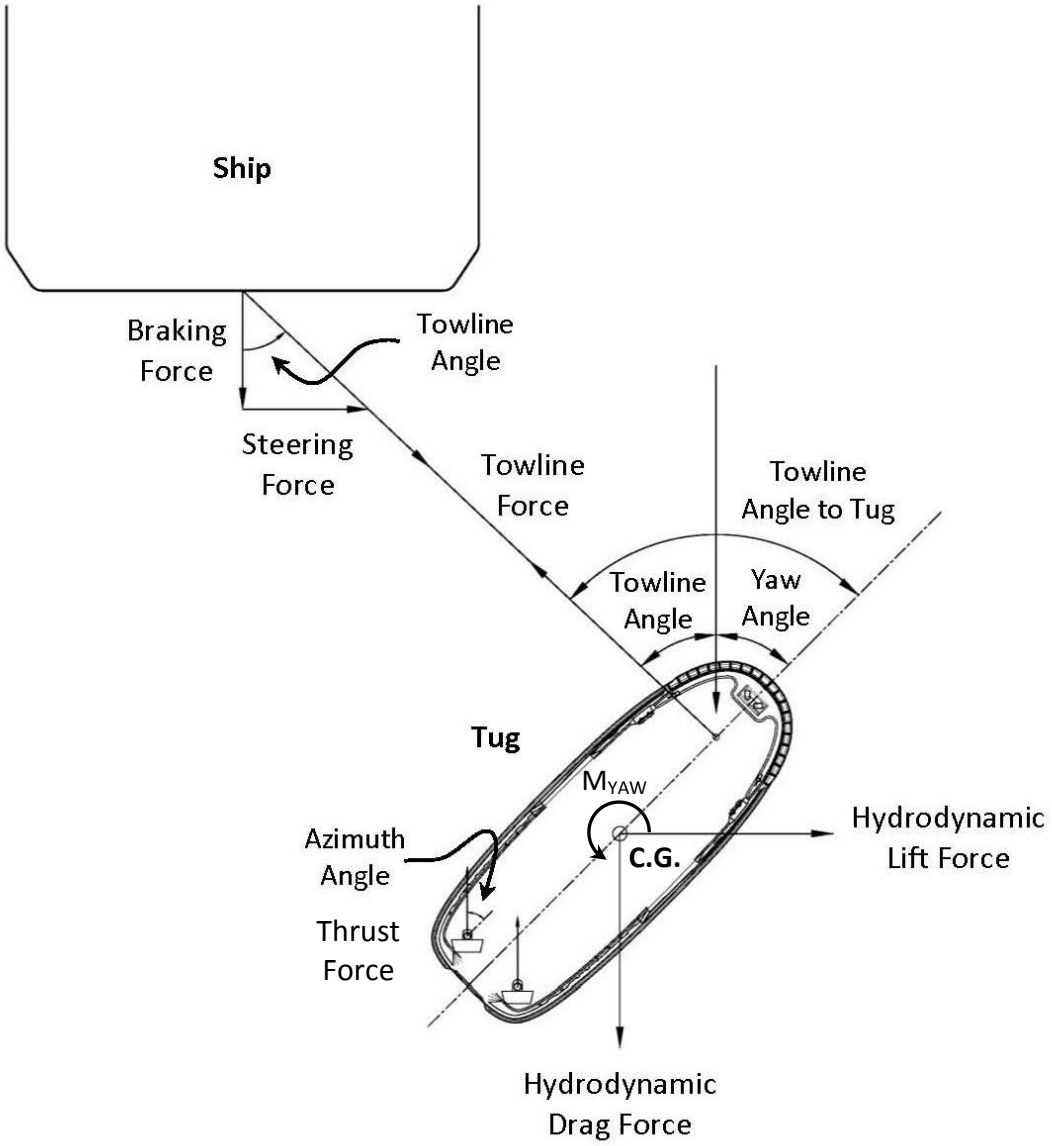

Figure 1.5: Diagram of Forces for Indirect Escort Operations

1.1.1 Direct Methods

The direct methods involve the tug being directly in line with the centerline of the escorted vessel. This method is used when only braking forces are required by the escorted vessel. The two direct methods are reverse arrest and transverse arrest.

Reverse arrest is when the drives operate at an azimuth angle of 180° and apply a force directly opposed to the direction of motion. The reverse arrest is most effective at speeds

from 0 to approximately 8 knots and can result in braking forces up to 1.5 times astern bollard pull, in which bollard pull refers to the maximum pulling force generated by a stationary vessel. (Jukola 1995).

Transverse arrest involves orienting the Z-drives perpendicular to the flow such that they are both propelling water outward at approximately 90°. Transverse arrest has been found to be a very effective method for providing stable braking forces at speeds above 8 knots. In transverse arrest, the braking force has been found to increase steadily as a function of advance speed (Jukola 1995).

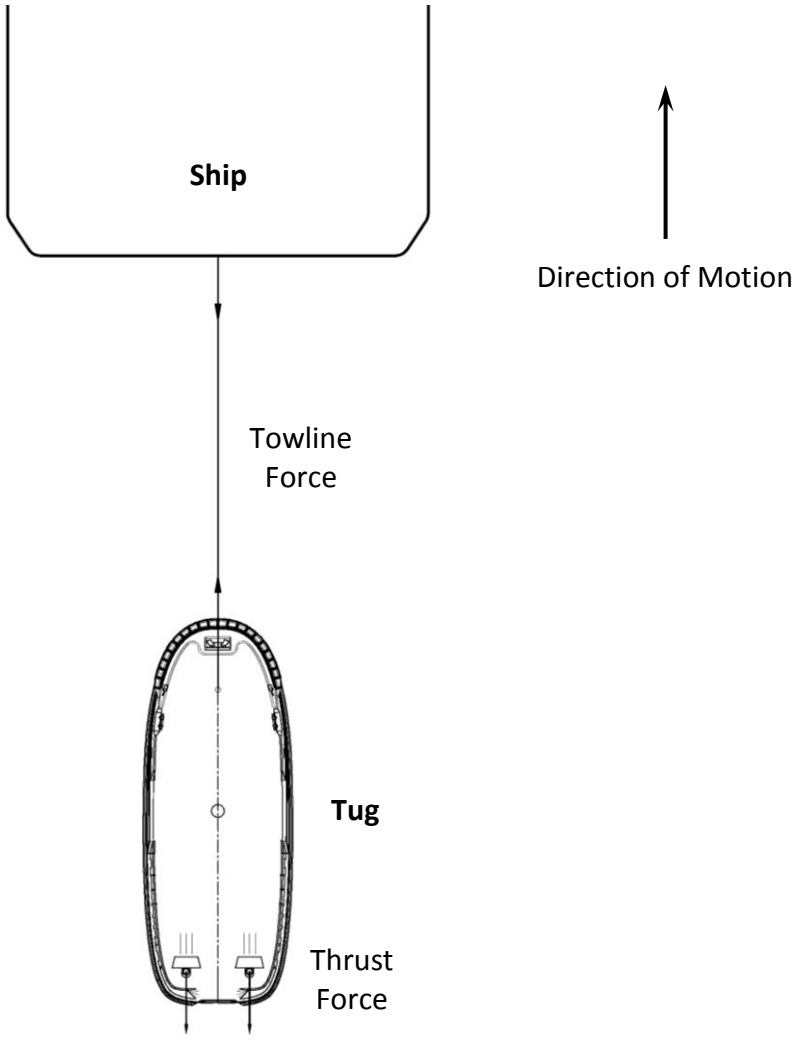

Figure 1.6: Escort Tug in Direct Mode

1.1.2 Indirect Methods

The indirect methods involve utilizing the hydrodynamic characteristics of the escort hull to generate lift and drag forces by orienting the tug at non-zero angles of attack to the flow. Indirect methods are generally used at speeds greater than 8 knots and often result in towline forces exceeding the vessel's rated bollard pull. The two modes of indirect escort operations are pure and powered indirect.

Pure indirect mode is when the tug thrusters apply a force perpendicular to the centerline of the tug resulting in a towline angle to the tug of approximately 90° as seen in Figure 1.7. Powered indirect mode consists of the tug utilizing all available engine power to provide the maximum possible steering forces. While pure indirect mode relies primarily on the hydrodynamic effects of the tug hull to create the steering and braking forces, powered indirect mode augments the hydrodynamic force with the thrusters to result in the highest steering forces (Brooks and Schisler, Suggested Tractor Command Language n.d.).

Typically, in an emergency situation in which the escorted vessel loses the ability to steer, transverse arrest would be utilized to slow the ship down and then the powered indirect mode would be used to then steer the vessel (Brooks, Escort Planning n.d.); however, the analysis of the maximum pure indirect steering and braking forces of a tug is crucial as it provides designers with a method of comparison to assess the escort performance of various hull and skeg geometries independent of the maximum available tug thrust.

A comparison of the escort tug positions relative to the escorted ship associated with pure and powered indirect is shown in Figure 1.7. It should be noted that the net thrust vector resulting from the Z-drives is not necessarily in-line with the drive orientation.

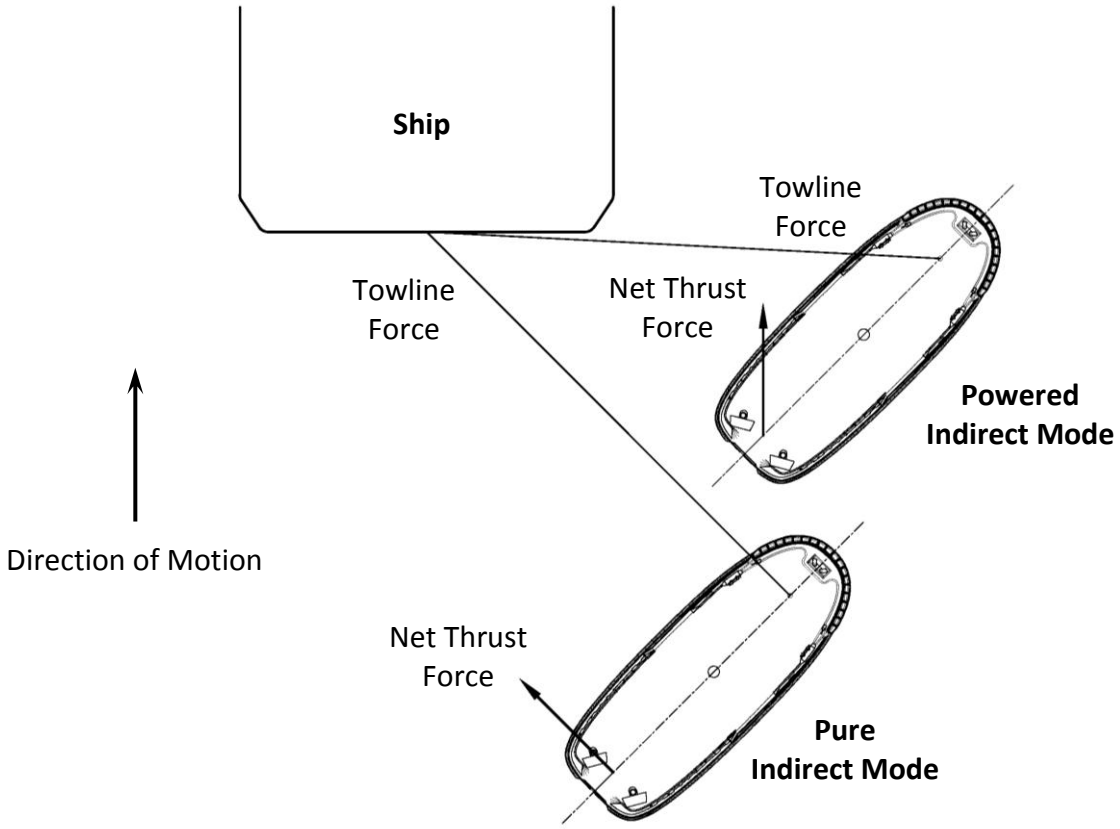

Figure 1.7: Comparison between Pure and Powered Escort Indirect Modes

1.2 Model Test Methods

The most established method used to analyze the performance of a ship hull is to carry out a series of resistance tests in a towing tank. Model tests can be conducted to measure the hull resistance for conventional vessel operations as well as the lift and drag forces of an escort tug in indirect mode. These forces can then be used to predict the escort performance.

1.2.1 Resistance

In order to calculate the resistance of a particular hull, a scale model of the hull is constructed. The model is then placed in a towing tank, ballasted to the desired draft and towed along the length of the tank with resistance continually measured. This procedure is repeated for several desired speeds in order to generate a resistance curve. The

measured model scale resistance values are then scaled up to full scale using a method described in Section 1.4, Scaling Methods.

1.2.2 Escort

The performance of an escort tug is determined by its maximum achievable steering force. To determine the maximum steering force experimentally the ship model is fitted with thrusters as well as a towline. One end of the towline is attached to the model in the location of the towing staple while the other is fixed to a towing carriage that runs the length of the towing tank. The Z-drives are set to full power and rotated incrementally through 360°. The towline force, towline angle, heel angle and yaw angle are recorded once equilibrium is achieved for each incremental azimuth angle.

While this method is simple and quick to carry out once the model and towing tank are prepared, it has significant disadvantages in terms of towing tank availability and cost. Towing tanks must be booked many months in advance and escort model tests can cost upwards of $100,000. In addition, significant changes to the hull of the tug are difficult to explore as individual models must be constructed ahead of the model tests. These limitations prevent a thorough performance analysis from being conducted on each new escort tug design.

1.3 CFD Methods

In recent years the model test approach has been overtaken by CFD ship performance studies. To illustrate the magnitude of this change, Figure 1.8 shows the shift in design tool usage from towing tank to CFD in the last fifteen years of American World Cup ship design. In the mid 1990's, the chief method of assessing ship performance was model testing in a towing tank. The practice of model testing began to decrease with the introduction of the numerical potential flow method, also referred to as the Panel Method. The foundational assumption in Panel Method is that the flow is inviscid and primarily influenced by velocity potential. The frictional resistance is then taken into account separately using flat-plate friction coefficients in conjunction with the hull wetted area.

The rapid improvement in computer technology and the emergence of commercial CFD codes resulted in CFD becoming the primary analysis tool used in the America's Cup design team.

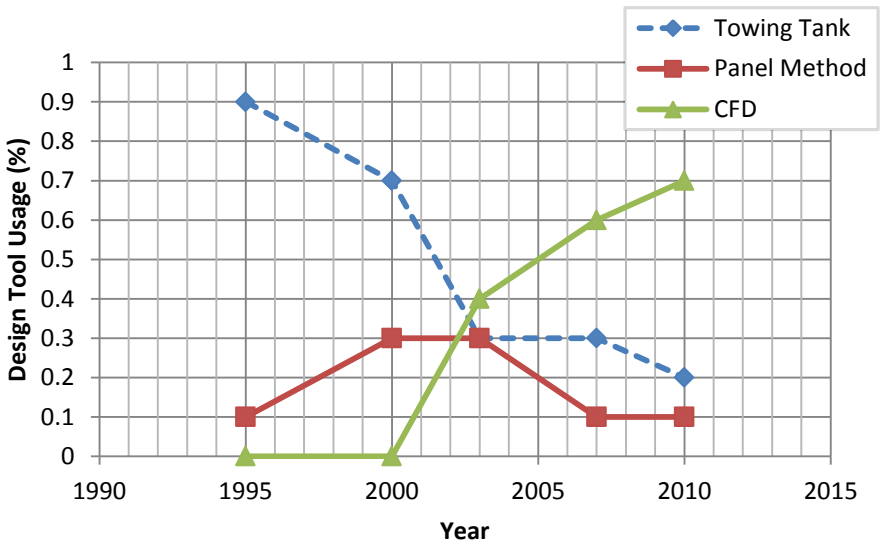

Figure 1.8: Proportional Design Tool Usage in Last 5 America's Cups (Viola, Flay and Ponzini 2011)

CFD has many advantages over model testing. These include but are not limited to, the ability to carry about full scale resistance and escort studies which eliminate errors associated with scaling effects, the capability of calculating pressure and shear force separately, as well as the flexibility to test several different hull configurations and conditions without the expense of having to construct several physical models.

CFD has also been applied to other marine problems such as predicting the motions and forces on various lifeboat designs being launched from a significant height into the water using an overset mesh (Morch, et al. 2008) as well as analyzing the scaling effects on form factor when predicting the performance of ships (Raven, et al. 2008). With the increased accessibility to commercial software packages and high powered computing, the use of CFD in solving both commercial and academic marine design problem is expected to increase substantially in the coming years. From studying the performance of

flume tanks on reducing ship roll to calculating ship resistance, CFD is set to permeate nearly every aspect of marine design process.

1.3.1 Resistance

The resistance studies undertaken in CFD are similar to those done in a towing tank. A mesh of the 3D hull form is created and placed within a virtual flow region. The fluid within the flow region surrounding the hull is prescribed a velocity and once convergence is achieved, the shear and pressure resistance is recorded for each desired velocity. It is common practice in the marine industry to perform the CFD resistance studies at model scale because of the significantly reduced computational time required. The model scale resistance results are then scaled to full scale resistance values using the same methods used in towing tank model test studies. The various methods of scaling the resistance results are shown in Section 1.4.

1.3.2 Escort

Currently there exists very little information on CFD escort studies to-date. One of the best documented cases of a CFD escort analysis was conducted by David Molyneux at Memorial University in Newfoundland (Molyneux and Bose 2007). In his analysis, Molyneux compared the hydrodynamic escort forces calculated using CFD to model tests conducted at the towing tank at the National Council's Institute for Ocean Technology. A hexahedral mesh was found to best predict the escort forces at high yaw angles (30 – 60°) resulting in calculated forces within 10% of those found in the model tests. The CFD study neglected the free surface affects and recommended including the free surface in future studies. The presence of the free surface will affect the hull wetted area and thus affect the frictional forces on the hull. Additionally, the wave buildup on the pressure side of the tug will influence the center of buoyancy and center of lateral pressure; therefore, changing the apparent escort tug hydrodynamic and hydrostatic characteristics.

1.4 Scaling Methods

Several different methods have been developed over the century to facilitate the scaling of resistance measured at model scale to full scale. To demonstrate the challenges associated with scaling measured force values the definition of resistance in the context of marine engineering as well as its components are outlined in the following section.

1.4.1 Resistance

The resistance of a vessel at a given speed is defined as, "the fluid force acting on the ship in such a way as to oppose its motion" and is "equal to the component of the fluid forces acting parallel to the [direction] of motion of the ship" (Harvald 1983). The total resistance of a ship is composed of several components. A comprehensive list of the components of resistance is provided in the following figure.

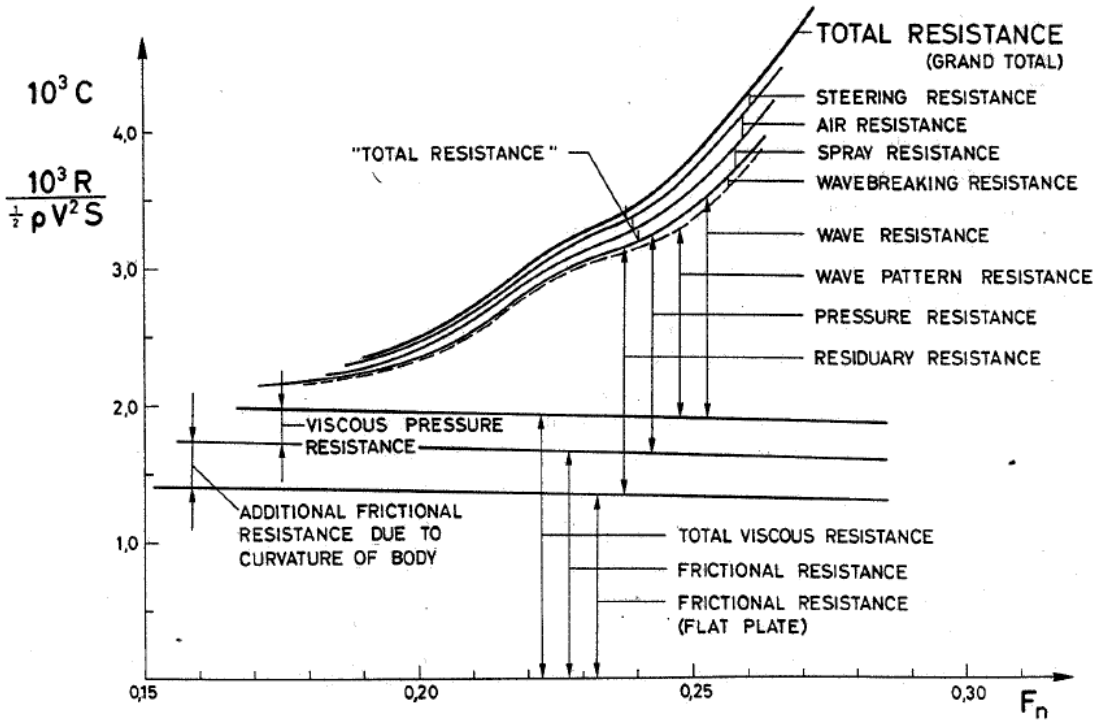

Figure 1.9: Components of Specific Resistance of Ships – Coefficient of Resistance versus Froude Number (Harvald 1983)

William Froude (Froude 1955) first proposed considering total resistance to be composed of two independent components: the frictional resistance and the residuary resistance. The frictional resistance is assumed to be due directly to the viscous forces and indirectly to the inertial forces as a result of changes to the vessel wetted area at higher flow velocities. The residuary resistance is due to the gravitational and inertial forces. The total resistance is the sum of the afore mentioned components.

$$R_T = R_F + R_R \quad \textbf{(1)}$$

Where R_T is the total resistance, R_F is the frictional component and R_R is the residuary component. The residuary resistance can be determined from the above equation if the frictional resistance is calculated separately. Several methods have been developed over the past 150 years to address problem of calculating the frictional resistance with the most common resistance scaling methods being:

- Froude's Method
- ITTC 1957 Method
- Hughes's Method
- Prohaska's Method
- ITTC 1978 Method

This paper will only describe Froude's method, as it is the basis for all other methods, and the ITTC 1957 method which is the most commonly used in towing tanks. Where each method differs is in the calculation of the frictional resistance. The ITTC 1957 uses a constant correlation line to determine the frictional resistance coefficient that is only a function of Reynolds Number. Hughe's, Prohaska's and the ITTC 1978 methods, use differing correlation lines that are a function of the ship geometry that is expressed as a form factor, k. Despite the fact these more modern methods generally provide better results, the older ITTC 1957 method remains the standard in many institutions primarily due to its simple application and consistency with others in the marine industry.

1.4.2 Froude's Method

Froude's method, as well as the ITTC 1957 method, assumes that the frictional resistance of the ship hull is similar to the resistance of a flat plate. Therefore, these methods are applicable if the hull is considered reasonably fine with little or no flow separation.

Froude's suggestion of considering resistance as the sum of frictional and residuary components has practical application when scaling model test results. If the frictional resistance is assumed to be independent of the residuary resistance, the following method can be used. It is first assumed that the residuary resistance is a function of the ratio of inertial to gravitational forces, as shown by the Froude Number in (2). Thus, in order to maintain the relative effect of the residuary resistance, the model test should be set up in such a way that it is conducted at the same Froude number expected in the full scale case. By assuming an equal Froude number between model and full scale cases, the Froude number equation shown below can be manipulated to determine the model scale velocity as shown in (2) and (3).

$$Fr = \frac{V}{\sqrt{gL}} \quad \textbf{(2)}$$

Where Fr is the Froude number, V is the free stream velocity, g is gravity and L is the waterline length of the ship.

$$V_M = \frac{V_S}{\sqrt{\lambda}} \quad \textbf{(3)}$$

Where V_M is the velocity at model scale, V_S is the velocity at full scale and λ is the scale factor. In the model test the total resistance is measured. In order to separate the frictional and residual components at least one of the components must be determined as evident from (4).

$$R_{TM} = R_{FM} + R_{RM} \quad \textbf{(4)}$$

Where R_{TM} is the total model scale resistance, R_{FM} is the model frictional resistance and R_{RM} is the model residuary resistance. Froude assumed that the frictional resistance is equal to the resistance of fluid flowing over a flat plate of an area corresponding to the waterline length of the ship multiplied by its mean girth. This area is referred to as the reduced wetted surface and is shown to provide more accurate friction resistance results than by using the actual hull wetted surface area [shown by Gutsche in 1933 (Lap 1956)]. With the ability to calculate the frictional resistance at both model and full scales, the residuary resistance can be isolated from the total model resistance. Because the residuary resistance is considered the component that is related solely to the Froude

number, it can be scaled in the following manner so long as the Froude numbers of the model and full scale cases are equal.

$$R_{RS} = \lambda_{\rho}\lambda_{L}^{3}R_{RM} \quad \textbf{(5)}$$

Where R_{RS} is the ship residual resistance, λ_{ρ} is the ratio of fluid densities from model and full scale conditions and λ_{L} is the model scale. By calculating the full scale frictional resistance using the flat plate assumption the total ship resistance is calculated from the following expression.

$$R_{TS} = R_{FS} + R_{RS} \quad \textbf{(6)}$$

Where R_{TS} is the total ship resistance, R_{FS} is the ship frictional resistance and R_{RS} is the ship residuary resistance.

1.4.3 ITTC 1957 Method

The ITTC 1957 method was proposed by the International Towing Tank Conference as a way to scale resistance results measured in a towing tank to full scale values and is currently the most used method in industry. The ITTC 1957 method utilizes all of the same assumptions as Froude's method with the addition of providing an explicit formula for calculating the model and ship frictional resistance coefficient as a function of the Reynolds number as shown in (7).

$$C_F = \frac{0.075}{(log_{10}R_n - 2)^2} \tag{7}$$

Where C_F is the frictional resistance coefficient and R_n is the Reynolds number found from waterline length and inflow velocity. The formula for calculating the total resistance coefficient is shown as:

$$C_{TM} = \frac{R_{TM}}{\frac{1}{2}\rho_M V_M^2 S_M} \tag{8}$$

Where C_{TM} is the model total resistance coefficient, ρ_M is the density of the fluid in the model test, V_M is the model scale velocity and S_M is the model wetted surface area. The model residuary resistance coefficient is then calculated by:

$$C_{RM} = C_{TM} - C_{FM} \tag{9}$$

Since the Froude number is the same for both the model and ship, it is assumed that the residuary resistance coefficients are equal.

$$C_{RS} = C_{RM} \tag{10}$$

The ITTC 1957 method then dictates that the total ship resistance coefficient is equal to

$$C_{TS} = C_{FS} + C_{RM} + C_A \tag{11}$$

Where C_A is the resistance coefficient representing the difference is hull roughness between the model and full scales. Most often C_A is set equal 0.0004 (Harvald 1983). The full scale ship resistance is then calculated by

$$R_S = C_{TS}\left(\frac{1}{2}\rho_S V_S^2 S_S\right) \tag{12}$$

Where R_S is the total ship resistance, ρ_S is the density of sea water, V_S is the ship speed and S_S is the ship wetted surface area. The ITTC 1957 method is shown graphically in the figure below.

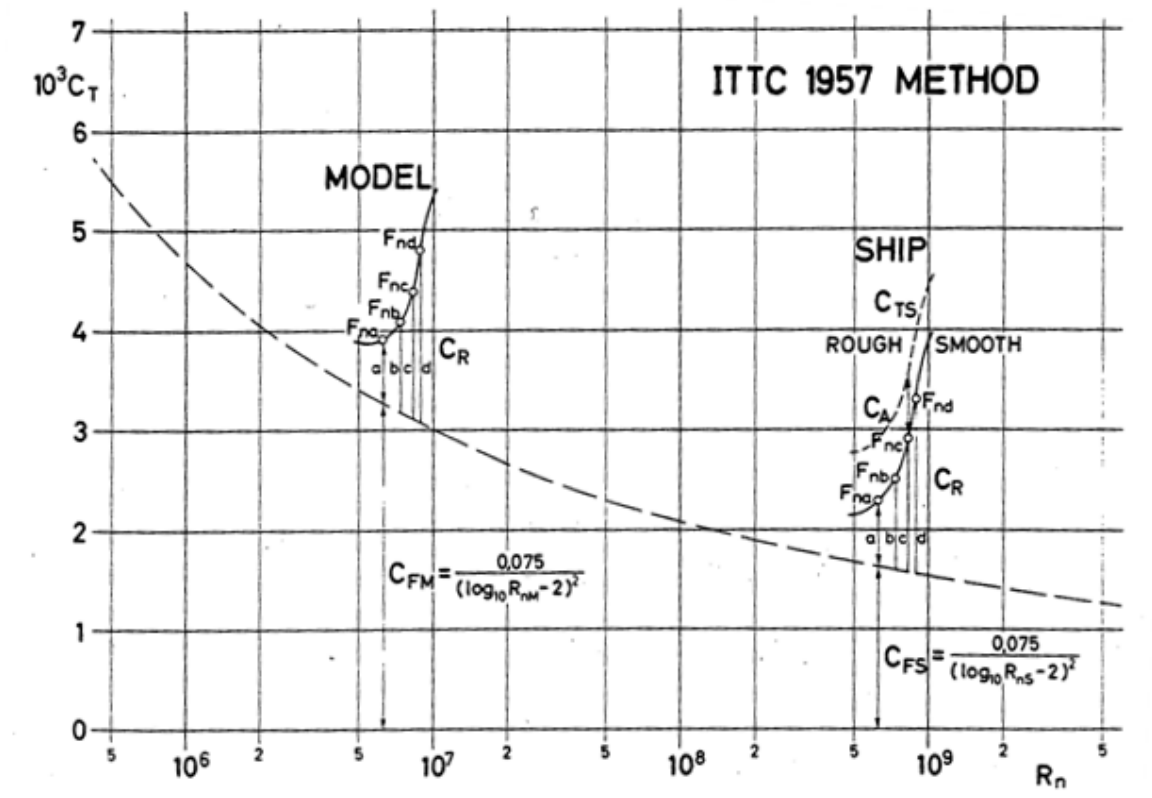

Figure 1.10: ITTC 1957 Resistance Coefficient Curve (Harvald 1983)

1.5 Objectives

The objectives of this thesis are threefold:

1. To outline and validate a CFD method for determining the hydrodynamic forces of an escort tug in indirect mode at a range of yaw angles from 0 to 90° at 8 knots;
2. To discuss the scaling effects on flow separation and vessel hydrodynamic forces by performing CFD studies on both model and full scale escort tugs in indirect mode; and,
3. To provide a method for converting the hydrodynamic forces of the CFD escort study into towline and thrust forces.

Chapter 2

Methodology

To achieve the previously mentioned objectives, the following two cases were considered:

Case 1: Full scale escort simulations at 8 knots from 0 to 90 degree yaw angles using the Robert Allan Ltd.'s *Irshad* hull form.

Case 2: 1:10 model scale escort simulations using the same hull form and range of yaw angles as the full scale study.

The selected full scale speed of the escort study was 8 knots as this is the speed where indirect escort forces surpass direct forces. Each case listed above utilized similar methodology. The following section outlines the coordinate system and CFD setup parameters such as mesh, boundary conditions, physics and discretization methods utilized in the CFD escort performance study.

2.1 Vessel Specifications

The vessel chosen for this study was the Robert Allan Ltd. designed *RAstar 3500* class escort tugboat, *Irshad*. The *RAstar* is a series of escort class tugboats with the proceeding number indicating the vessel's length, in this case 35 meters. The *Irshad* was selected for this study primarily because of the significant model test data available on this hull and because it is considered to be a high performance escort tug.

The three most important factors that influence the escort performance of a vessel are the staple, propulsion, and hull and skeg geometry. The hull and skeg geometry directly determine the center of lateral resistance. The relative position of the drives and staple to the center of lateral resistance, as illustrated in Figure 2.1, have a significant effect on the maximum achievable steering force as well as the vessel's escort stability.

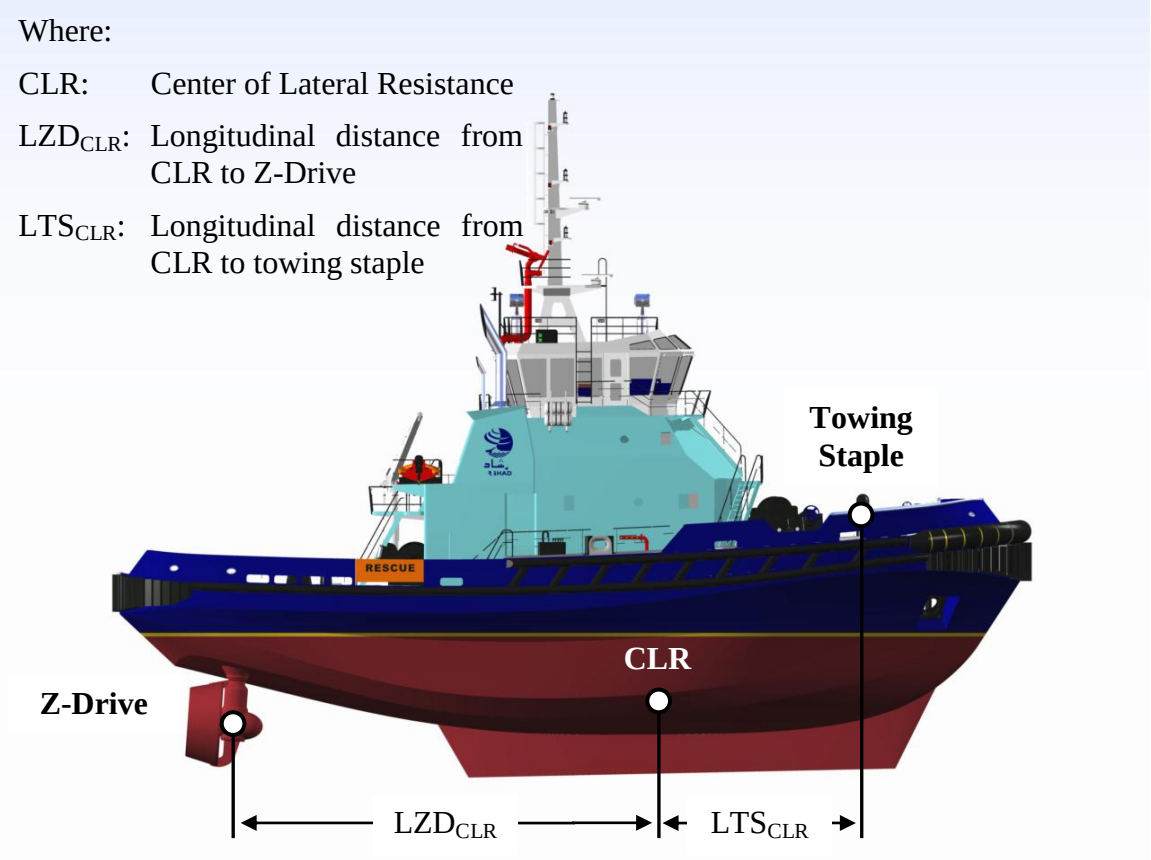

Figure 2.1: *RAstar 3500* ASD Escort Tug *Irshad* – Profile

2.2 Software

The commercial CFD code, *STAR-CCM+* version 6.04.014 by CD-adapco, was utilized for the escort CFD study described in this thesis. *STAR-CCM+* was chosen because it is the CFD software currently used by Robert Allan Ltd. and it contains a six degree of freedom (6 DOF) motion solver as well as a robust built-in automated mesh generator.

The algorithm utilized in the CFD code *STAR-CCM+* uses a Semi-Implicit Method for Pressure-Linked Equations (SIMPLE) approach to account for the relationship between the pressure and velocity field in the solver domain. The SIMPLE algorithm involves the following steps (Versteeg and Malalasekera 1995):

1. Set a guessed initial pressure field for the entire region based on the preset boundary conditions;

2. Compute the velocity components for the entire region using the guessed pressure field;
3. Solve the pressure correction equation to determine the corrected pressure field;
4. Solve the corrected velocity field using the corrected pressure field; and finally,
5. If flow is compressible, update the density due to pressure changes.

The SIMPLE algorithm is used in conjunction with the Segregated Flow Solver as an alternative to solving fully coupled equations for the velocity and pressure. It is well suited to constant density problems at low Mach numbers.

2.3 Governing Equations

The algorithm used by *STAR-CCM+* is based on the finite-volume (FV) method which involves subdividing the 3D domain into a region of interconnected individual control volumes (CVs). The control volumes are typically made smaller and more densely concentrated in areas of rapidly changing flow, and are larger and less densely concentrated in the far-field. The governing equations are discretized from their integral form using a second order upwind approximation in space and a first order central differencing method in time. The flow is assumed to be governed by the Reynolds-averaged Navier-Stokes equations with turbulence effects accounted for with an eddy-viscosity model. There are five governing equations solved for each iteration of the CFD simulation. These equations consist of the mass conservation equation, the three momentum conservation equations and the two equations for turbulence properties assuming k-ω or k-ε models are chosen.

Mass conservation:

$$\frac{\mathrm{d}}{\mathrm{d}t}\int_V \rho \mathrm{d}V + \int_S \rho(\mathbf{v}-\mathbf{v}_\mathrm{b})\cdot\mathbf{n}\mathrm{d}S = 0 \qquad \textbf{(13)}$$

Momentum conservation:

$$\frac{\mathrm{d}}{\mathrm{d}t}\int_V \rho\mathbf{v}\mathrm{d}V + \int_S \rho\mathbf{v}(\mathbf{v}-\mathbf{v}_\mathrm{b})\cdot\boldsymbol{n}\mathrm{d}S = \int_S (\mathbf{T}-p\mathbf{I})\cdot\mathbf{n}\mathrm{d}S + \int_V \rho\mathbf{b}\mathrm{d}V \qquad \textbf{(14)}$$

Generic transport equation for k-ε or k-ω turbulence model:

$$\frac{\mathrm{d}}{\mathrm{d}t}\int_V \rho\phi \mathrm{d}V + \int_S \rho\phi(\mathbf{v}-\mathbf{v}_\mathrm{b})\cdot\boldsymbol{n}\mathrm{d}S = \int_S \Gamma\nabla\phi\cdot\mathbf{n}\mathrm{d}S + \int_V \rho b_\phi \mathrm{d}V \qquad \textbf{(15)}$$

Where in the above equations, ρ is the fluid density, **v** is the fluid velocity vector, $\mathbf{v}_\mathrm{b}$ is the velocity of the CV surface of area *S*, **n** is the unit vector normal to the CV surface, *V* is the volume of the CV, **T** is the stress tensor in terms of the velocity gradients and eddy viscosity, *p* is the pressure at the CV, **I** is the unit tensor, φ is the scalar variable *k*, ε, or ω depending on the selected turbulence model, Γ is the diffusivity coefficient, **b** is the body force vector per unit mass and b_φ is the source or sink value for φ. The terms from left to right are the transient term, the convective flux, the diffusive flux, and the volumetric source term.

To utilize the 6 DOF solver embedded in *STAR-CCM+* the problem must be considered unsteady in which the equations listed above are solved for several iterations until convergence is achieved at the current time. These iterations completed within each time step will hence-forth be referred to as inner-iterations. When the inner-iterations complete, the solution is stepped in time at the prescribed time step with the new position of the body determined by the space-conservation law shown below.

$$\frac{\mathrm{d}}{\mathrm{d}t}\int_V \mathrm{d}V - \int_S \mathbf{v}_\mathrm{b}\cdot\mathbf{n}\mathrm{d}S = 0 \qquad \textbf{(16)}$$

2.4 Coordinate System

For future reference a standard vessel right-hand coordinate system is shown in Figure 2.2. The forces and moments about each axis were calculated for each pre-set yaw angle. The CFD simulation was fixed in the X and Y directions and released to heave in the Z direction.

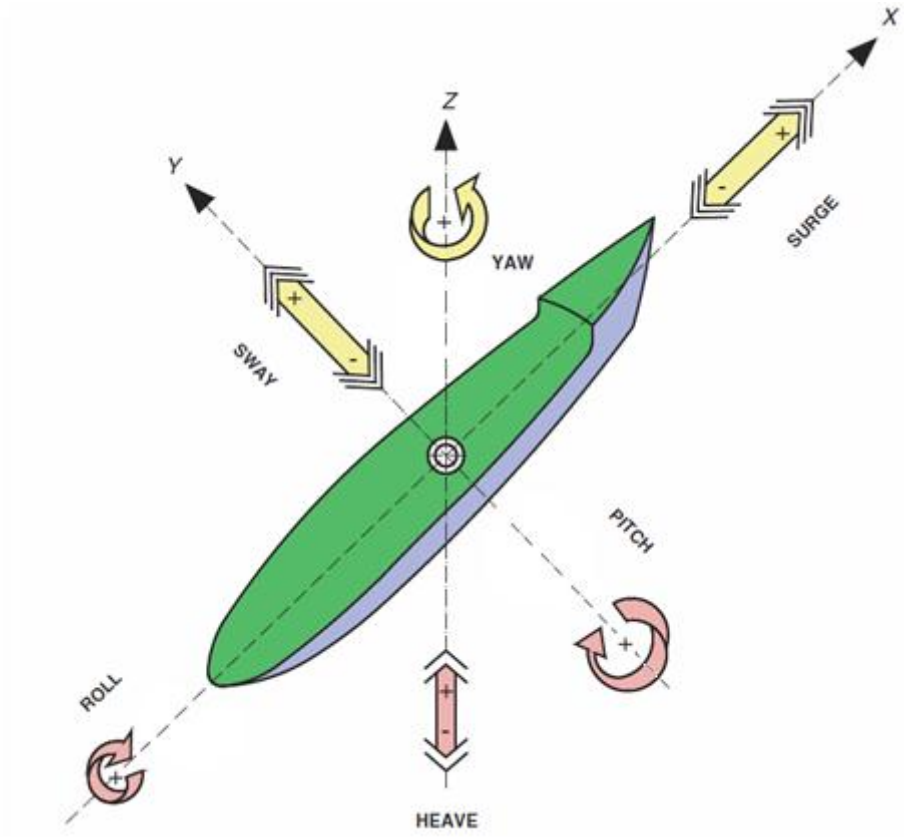

Figure 2.2: Ship Coordinate System (Baniela 2008)

The free body diagram of an escort tug in indirect mode is shown in Figure 2.3.

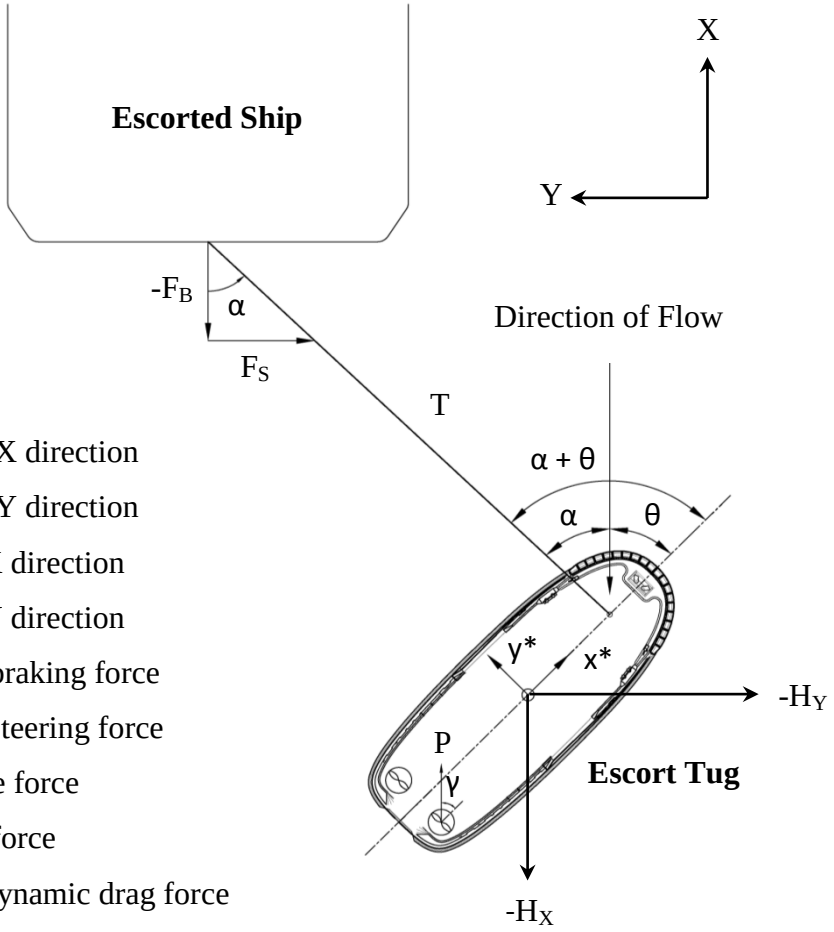

Where:

X :	Global X direction
Y :	Global Y direction
x*:	Local X direction
y*:	Local Y direction
F_B :	Escort braking force
F_S :	Escort steering force
T :	Towline force
P :	Thrust force
H_X :	Hydrodynamic drag force
H_Y :	Hydrodynamic lift force
α :	Towline angle
θ :	Yaw angle
γ :	Thrust angle

Figure 2.3: Free Body Diagram and Coordinate System of Escort Tug in Indirect Mode

The global coordinate system corresponds to the direction of flow with X pointed in the direction of the escorted ship's motion. The local coordinate system is aligned with the escort tug with the X component directed along the longitudinal axis of the ship, the Y component pointing port and the Z component pointing up.

2.5 Flow Region and Boundary Conditions

The three dimensional flow region used in this study was the same for all three cases. The flow region was represented by a box with relative dimensions shown in Figure 2.4 and Figure 2.5.

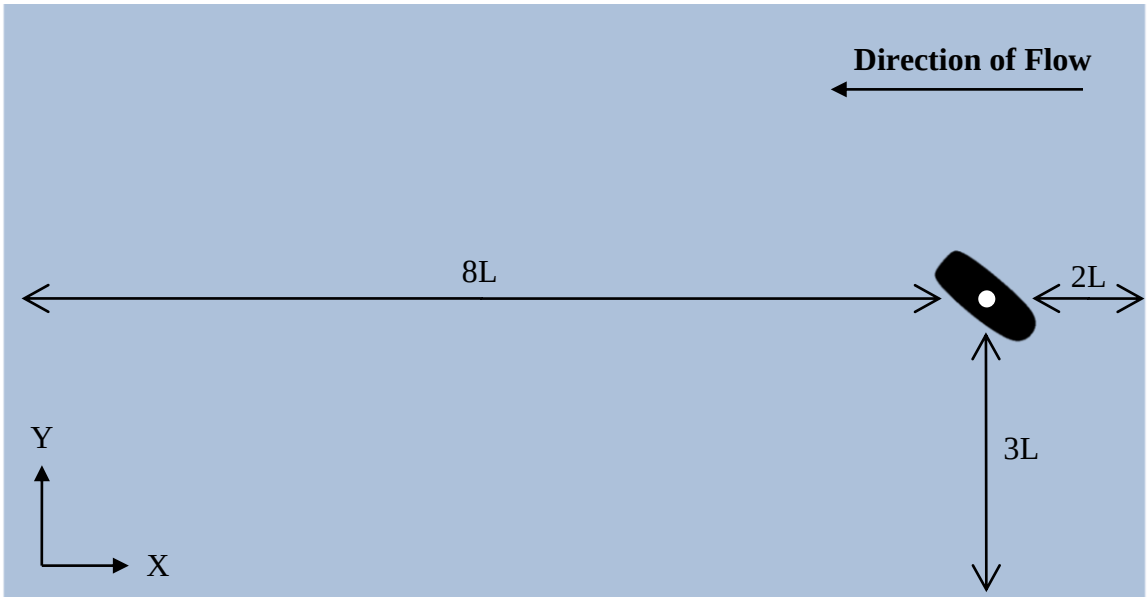

Figure 2.4: Flow Region - Plan View

Figure 2.5: Flow Region - Profile View

The dimensions of the flow domain were determined through recommended best practices in CFD marine resistance prediction by the STAR-CCM+ developed, CD-adapco. The domain size was deemed appropriate after visualizing velocity gradients from the tug to the boundaries to ensure no discontinuities existed.

The same boundary conditions were used for all three cases. The following figure and table define each boundary by name and type.

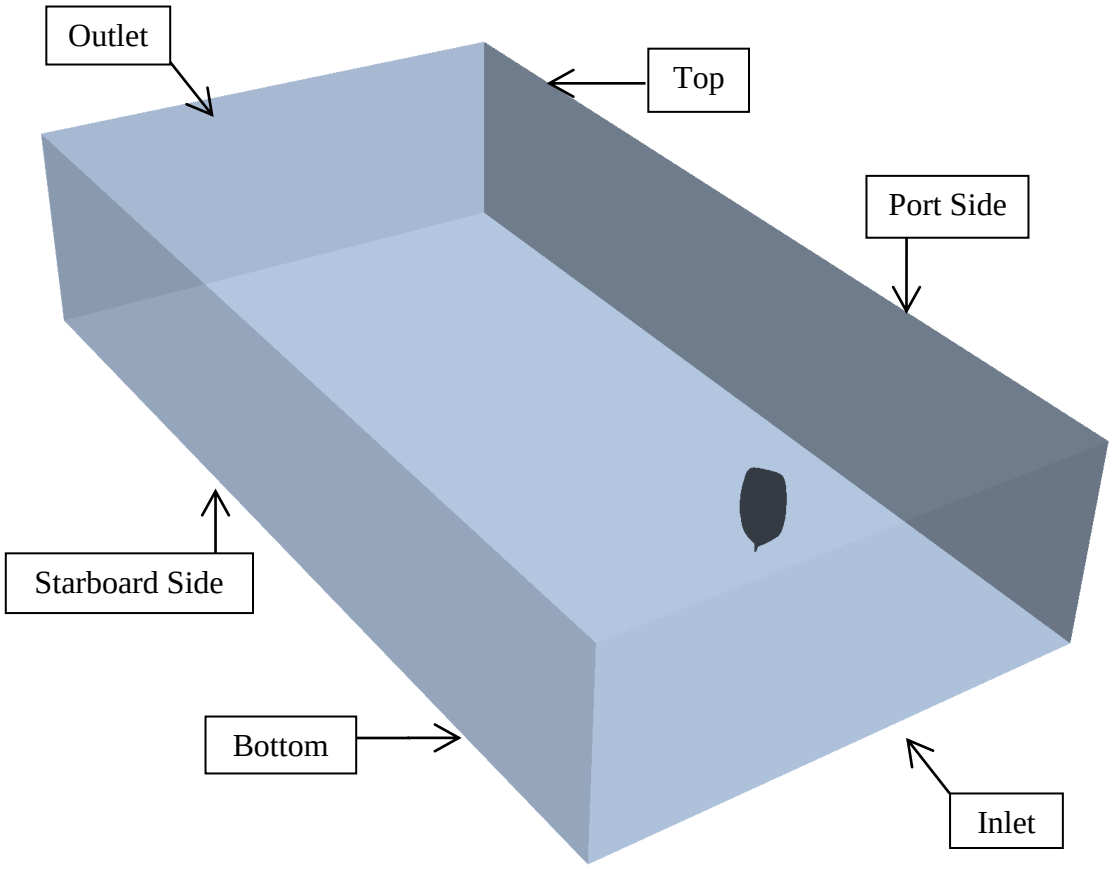

Figure 2.6: Flow Region with Defined Boundary Conditions

Each boundary condition shown in Figure 2.6 is listed along with its condition in the table below.

Table 1: Boundary Conditions

Name	Type
Inlet	Velocity Inlet
Starboard Side	Velocity Inlet
Port Side	Velocity Inlet
Top	Velocity Inlet
Bottom	Velocity Inlet
Outlet	Pressure Outlet

The velocity inlet condition prescribes a set velocity vector equal to the inflow condition. By setting the sides, top and bottom to this condition it was important to make the flow

region wide enough for the viscous damping effects of the fluid to dampen the generated waves prior to reaching the boundaries. The boundary conditions were selected based on the standard practice at Robert Allan Ltd. The choice of boundary condition was not found to have a significant impact on the vessel hydrodynamic forces and moments.

2.6 Mesh

The solution of any CFD problem is dependent on the existence and quality of the generated mesh. The meshing process of this study involved the following steps: Firstly, the surface mesh representing the hull of the escort tug was imported, secondly the imported mesh was repaired to ensure its suitability for re-meshing, and, lastly, the volume mesh used for the solution process was generated. Once a volume mesh was generated, a mesh independence study was conducted, discussed in Section 3.1, to assess the sensitivity of the results to the chosen mesh density.

2.6.1 Import Mesh

The hull forms of the escort tugs utilized in this study were provided by Robert Allan Ltd. and initially created in the lines fairing program, *FastShip*. The following steps describe the process followed for each mesh utilized in this study.

1. Escort tug hull lines faired in *FastShip* based on vessel requirements;
2. *FastShip* hull lines imported into *Rhino3D* to create an enclosed, 3D hull model;
3. Stereolithography (STL) mesh of the hull created in *Rhino3D*; and,
4. STL mesh imported into *STAR-CCM+*.

2.6.2 Surface Mesh Repair

Once the STL mesh was imported into *STAR-CCM+* it was necessary to repair the mesh to ensure its suitability for re-meshing. The surface mesh imported from *Rhino3D* often has pierced and high aspect ratio cells that must be corrected prior to the creation of the volume mesh. An example of a mesh imported from *Rhino3D* into *STAR-CCM+* is shown in Figure 2.7.

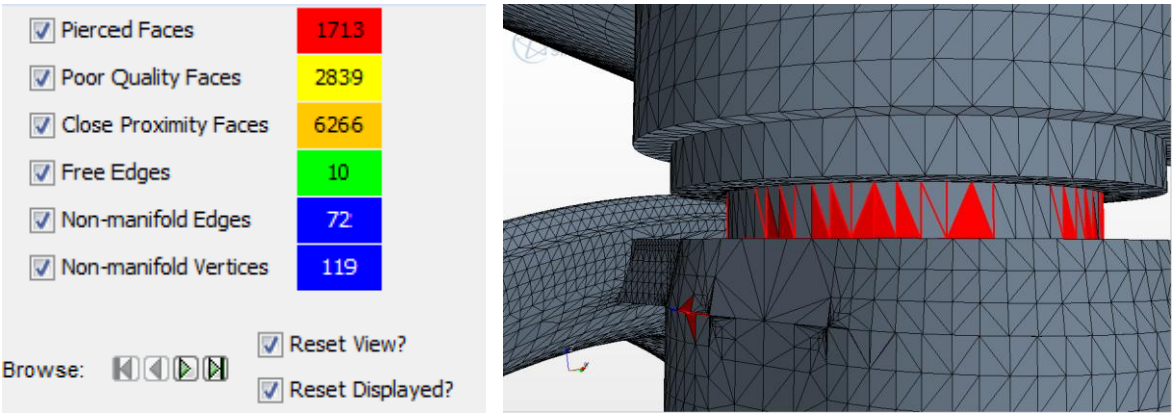

Figure 2.7: Example of an Imported STL mesh

Once all of the pierced faces, free edges, non-manifold edges and non-manifold vertices have been eliminated the surface mesh was considered adequate.

2.6.3 Volume Mesh

Due to the nature of the CFD simulation, a three dimensional volume mesh is required for the proper discretization of the domain. *STAR-CCM+* utilizes an automatic volumetric mesh generator that can create a hexahedral, tetrahedral, or polyhedral mesh. The volume mesh used in this study is composed of hexahedral cells that are trimmed at the surface mesh representing the escort tug hull. Volumetric controls are used to refine the mesh in areas of rapidly changing flow, such as around the skeg and in the wake of the tug. An example volume mesh for an escort tug simulation is shown below.

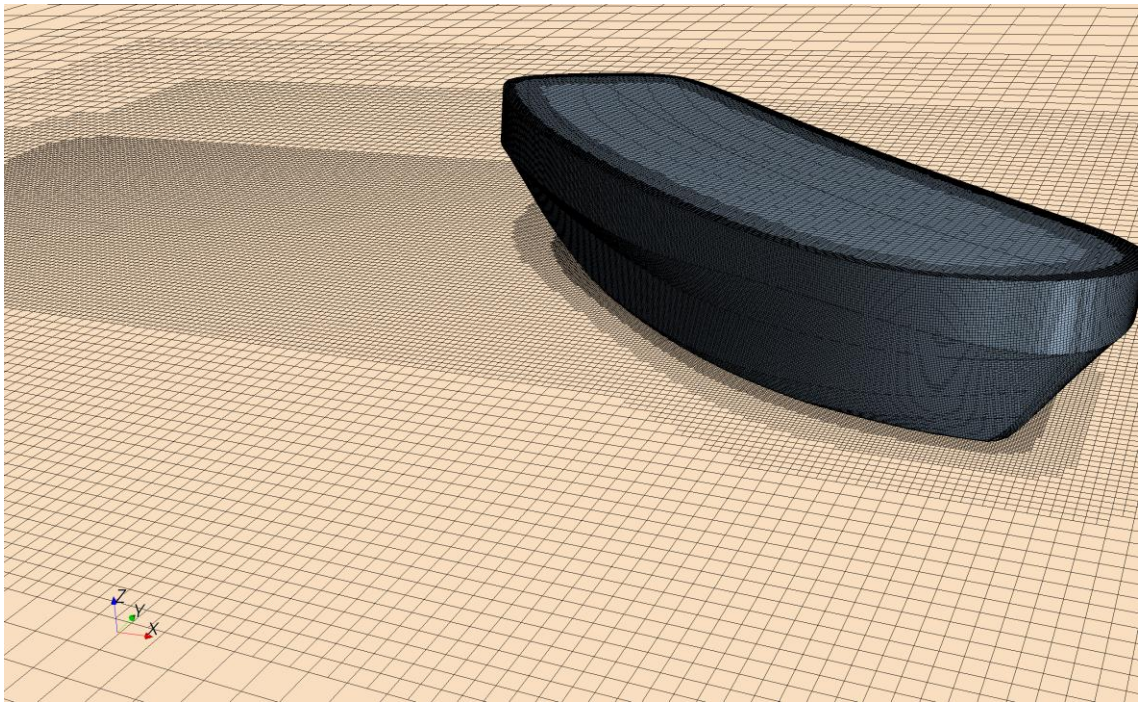

Figure 2.8: Escort Tug Volume Mesh Wake Refinement

In order to reduce the blockage effects of the boundaries in the simulation, the volume mesh is coarsened downstream and to either side of the hull to dampen out the formation of waves. The goal is to have no waves reach the boundaries as to eliminate any reflected waves that may influence the hydrodynamic forces on the hull. Figure 2.9 shows an example volume mesh used for the 45 deg yaw model scale simulation.

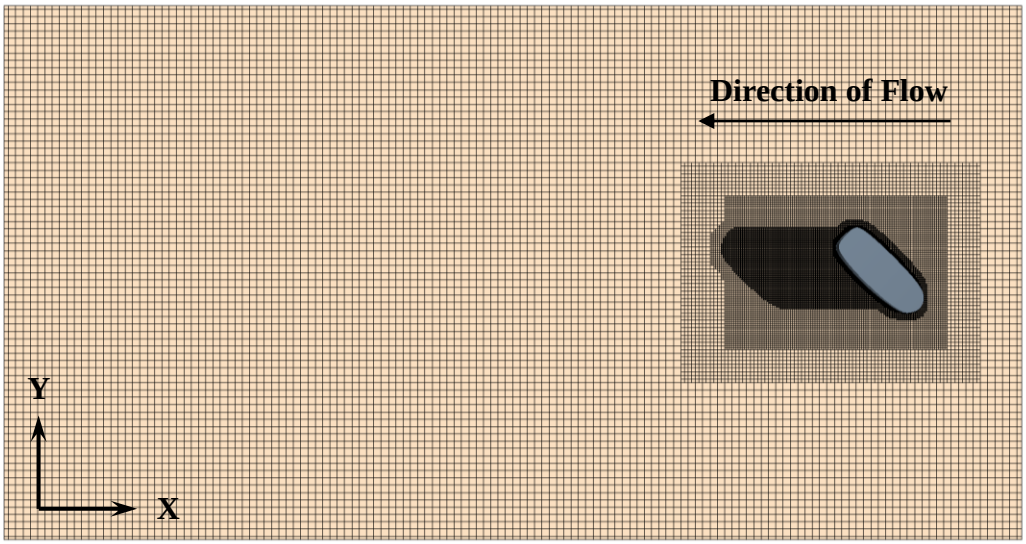

Figure 2.9: Example Flow Region Volume Mesh for Model Scale Simulation

A complete list of the meshing values used for each case in this study is included in the appendix with a summary of values shown in the table below.

Table 2: Summary of Volume Mesh Parameters

Parameter	Units	Full Scale	1:10 Model Scale
Base Size	m	5.0	0.5
Template Growth Rate		Slow	Slow
Hull Surface Size(1)	%	1.56	3.125
Deck Surface Size(1)	%	10	12.5

(1) Meshing parameter given as a percentage of base size

2.6.4 Prism Layer Mesh

STAR-CCM+ uses what is referred to as a prism layer mesh to calculate the flow against a surface. A prism layer mesh is composed of hexahedral cells aligned parallel to the hull surface. For this study the Two-Layer Realizable k-ε turbulence model was used; therefore, the thickness of the first cell against the surface was restricted by the Law of the Wall. The Law of the Wall states that the average velocity of turbulent flow near a wall is related to the distance away from the wall. As shown in Figure 2.10, there are three regions of the boundary layer where the relationship between velocity and wall distance change. In Figure 2.10, u^+ represents the dimensionless velocity and y^+ represents the dimensionless distance from the wall, defined in equations (21) and (22) below. In the Viscous Sublayer from y^+ 1 to 5, there exists a linear relationship between the velocity and the wall distance. A logarithmic relationship exists for u^+ at y^+ values greater than 30. The Buffer Layer is the region between the Viscous Sublayer and the Logarithmic Region that continuously joins the other two layers. For the selected Two-Layer Realizable k-ε turbulence model to adequately approximate the boundary layer the boundary mesh must resolve the flow to a y+ of 50 (CD-adapco 2011).

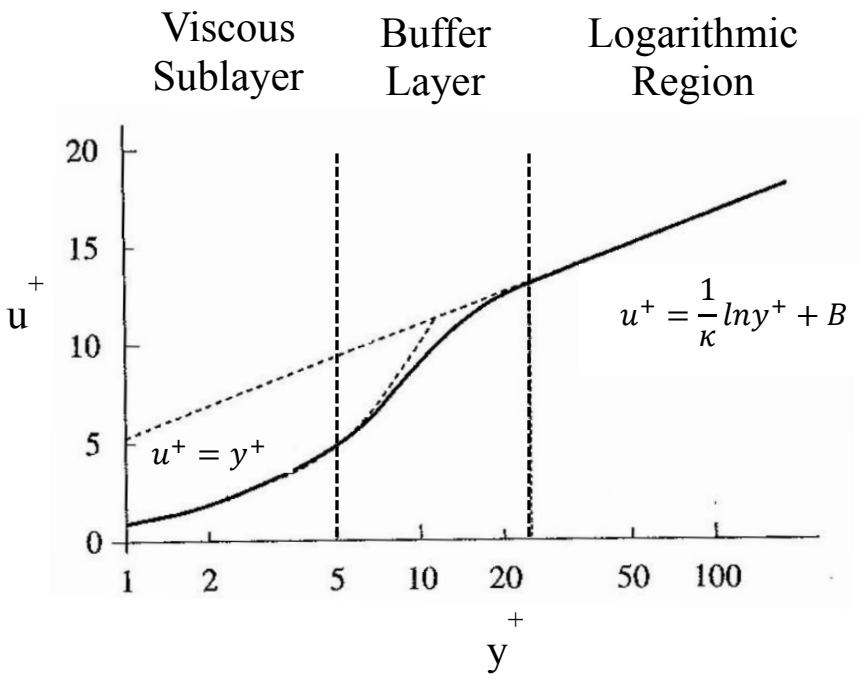

Figure 2.10: Law of the Wall (Schlichting and Gersten 2000)

The near wall thickness of the first prism layer cell to achieve a y+ value of 50 was calculated by the following procedure. Firstly, the model scale equivalent velocity must be determined if applicable. This was accomplished by assuming a constant Froude number between scales as shown in the following series of equations.

$$\frac{V_s}{\sqrt{gL_s}} = F_R = \frac{V_m}{\sqrt{gL_m}}$$

$$Let\ \lambda = \frac{L_s}{L_m}$$

$$\therefore V_m = V_s\sqrt{\frac{1}{\lambda}} \qquad \textbf{(17)}$$

Where V_s and V_m are the ship and model scale velocities respectively, g is gravity, L_s and L_m are the ship and model scale waterline lengths respectively, and Fn is the Froude number. Secondly, the Reynolds number was determined by:

$$Rn_L = \frac{\rho VL}{\mu} \qquad \textbf{(18)}$$

Where Rn_L is the Reynolds number, ρ is the fluid density, V is the free stream velocity, L is the wetted ship length and μ is the fluid viscosity. Thirdly, in order to estimate the wall

shear stress, the friction along the ship hull was considered analogous to a flat plate with a friction coefficient represented by:

$$C_f = \frac{2 * 0.036}{Re_L^{1/5}} \quad \textbf{(19)}$$

Fourthly, the mean wall shear stress was determined by the following relation.

$$\tau_w = \frac{1}{2}\rho V^2 \overline{C_f} \quad \textbf{(20)}$$

Finally, the friction velocity was found from equation (21), and the wall y value was found using the *Law of the Wall* (Schlichting and Gersten 2000) relation shown in equation (22):

$$u^* = \sqrt{\frac{\overline{\tau_w}}{\rho}} \quad \textbf{(21)}$$

$$y = \frac{y^+ \mu}{u^* \rho} \quad \textbf{(22)}$$

The wall y value was then used to determine the first prism layer thickness to satisfy the y+ criteria necessary for the 2-layer turbulence model. Since the finite volume method solves the discretized equations for a finite control volume, the first prism layer cell must have its center at a distance of y from the ship surface. Therefore the first prism layer thickness was determined by:

$$t = 2 * y \quad \textbf{(23)}$$

Because of the difference in velocity and ship length between the full scale and model scales cases, different near wall prism layer thicknesses were used. The following table outline the prism layer conditions used for the full scale and model scale cases.

Table 3: Summary of Prism Layer Mesh Parameters

Prism Layer Parameter	**Units**	**Full Scale**	**1:10 Model Scale**
Number of Prism Layers		7	5
Overall Prism Layer Thickness	m	0.05	0.025
Near Wall Prism Layer Thickness[(1)]	mm	0.971	2.17

[(1)] Value determined by procedure described above

While the previously discussed method provides an adequate process for sizing the near wall prism layer, it can often result in very small y values in full scale simulations due to the high Reynolds numbers. Small 'y' values at the hull surface result in very large cell aspect ratios in the volume mesh which lead to simulation stability problems.

2.7 Physics

STAR-CCM+ has a significant library of various physics models that enable many physical heat-transfer and fluid flow problem to be solved. The following table outlines the key physics models chosen for this project.

Table 4: Summary of Physics Parameters

Parameter	**Value**
Space	Three Dimensional
Time	Implicit Unsteady
Material	Eulerian Multiphase Mixture
Multiphase Flow Model	Volume of Fluid (VOF)
Viscous Regime	Turbulent
Turbulence Model	Realizable K-Epsilon Two-Layer Model

The two phases used were salt water and air with the following properties.

Table 5: Phases

Phase	**Density (kg/m^3)**	**Dynamic Viscosity (Pa-s)**
Salt Water	1025	$1.21*10^{-3}$
Air	1.184	$1.855*10^{-5}$

The water level and fluid velocity were set using the STAR-CCM+ physics parameter Volume of Fluid (VOF) Waves. The VOF method handles two-phase flow by assigning a volume fraction of fluid value to every cell. To the cells below the specified waterline, the volume fraction of water was set to 1.0 and the volume fraction of air was set to 0.0. The cells above the waterline were assigned the opposite volume fraction values. The free surface was defined by the cells with a volume fraction of water and air equal to 0.5.

The water level was set to correspond with a full scale vessel draft of 4.04 m. The wave velocity was set to correspond with a full scale speed of 8 knots. For the model scale simulation the velocity was scaled using equation (3).

2.8 Turbulence Model

The turbulence model used in this study was the Realizable k-ε two-layer model (Shih, et al. 1994). The Realizable k-ε was found to produce slightly more accurate results when predicting the resistance of floating bodies (Peric, et al. 2008) when using *STAR-CCM+*. The realizable model has been shown to be better suited to many physical problems (CD-adapco 2011) and is combined with the two-layer approach, which switches to a one-equation model for low y+ values (Rodi 1991), to ensure it is valid for all y^+ values. The k-ε turbulence model is commonly used in the marine CFD industry for resistance calculations and yields nearly identical results to the k-ω for favourable pressure gradients with little or no flow separation (Viola, Flay and Ponzini 2011).

2.9 Discretization

Different discretization schemes were used for the transient, convective, source and diffusion terms in the governing equations.

2.9.1 Transient

A first order temporal scheme, also known as Euler Implicit, was used to discretize the transient terms in the governing equations (CD-adapco 2011).

$$\frac{d}{dt}(\rho\phi V)_0 = \frac{(\rho_0\phi_0)^{n+1} - (\rho_0\phi_0)^n}{\Delta t} V_0 \qquad \textbf{(24)}$$

Where φ is the scalar term for v, *k* or ε. The Euler Implicit discretization uses the solution at the current time level, *n+1* and at the previous time level, *n*.

2.9.2 Convective

The convective flux at each cell face was determined using a second-order upwind discretization scheme shown in the following expression (CD-adapco 2011).

$$(\dot{m}\phi)_f = \begin{cases} \dot{m}_f \phi_{f,0} & \text{for } \dot{m}_f \geq 0 \\ \dot{m}_f \phi_{f,1} & \text{for } \dot{m}_f < 0 \end{cases} \quad \textbf{(25)}$$

Where the scalar face values, $\phi_{f,0}$ and $\phi_{f,0}$ were determined by interpolating the neighbouring cell values shown below.

$$\phi_{f,0} = \phi_0 + s_0 \cdot (\nabla\phi)_{r,0}$$
$$\phi_{f,1} = \phi_1 + s_1 \cdot (\nabla\phi)_{r,1} \quad \textbf{(26)}$$

Where $(\nabla\phi)_{r,0}$ and $(\nabla\phi)_{r,1}$ are the limited reconstruction gradients in the neighbouring cells 0 and 1 respectively (CD-adapco 2011). The definitions for s_0 and s_1 are shown as follows:

$$s_0 = x_f - x_0$$
$$s_1 = x_f - x_1 \quad \textbf{(27)}$$

The second-order upwind differencing scheme was used because it has higher order accuracy than the first-order method and still results in a converged solution.

2.9.3 Source

The source term in the governing equation was discretized as follows:

$$\int_V \rho \mathbf{b} \mathrm{d}V = (\rho \mathbf{b} V)_0 \quad \textbf{(28)}$$

The above relationship is a simple, second-order approximation for a finite volume cell 0 (CD-adapco 2011).

2.10 Solver

The selected time step varied with ship scale. The full scale simulations had a time-step ranging from 0.02 seconds to 0.03 seconds. The model scale simulations had a time-step ranging from 0.03 to 0.05 seconds.

2.11 Studies

Three classifications of simulations were conducted in this study: grid study, validation and indirect escort tug performance analysis. The grid studies consist of a 0 degree yaw

angle model scale study and a 40 degree yaw angle full scale study. The validation study consisted of two parts: resistance and escort. The resistance validation involved comparing CFD data to resistance model test data for the *RAstar 3500, Irshad*. The escort validation involved comparing CFD and model test data for an escort hull studied by David Molyneux in Newfoundland (Molyneux and Earle 2001). The indirect escort performance analysis involved calculating the body forces and moments of the tug by running a series of CFD simulations at various angles of attack, or yaw angles. The complete list of simulations conducted for each classification is provided in the following sections.

In each study, the Dynamic Fluid Body Interaction (DFBI) solver in *STAR-CCM+* was used to handle the dynamic motion of the tug. The solver allows the user to fix or free the x, y and z translation and rotation degrees of freedom. For all of the studies completed in this research, the tug was only free to heave (z-translation) with all other directions fixed.

2.11.1 Grid Studies

Two grid independence studies were conducted. The first grid study was conducted at a 0 degree yaw angle at 1:10 model scale. Four simulations were run with mesh sizes of 50%, 75%, 100% and 125% relative to the model scale base size given in Table 2. The second grid study consisted of an escort tug at a 40 degree yaw angle with mesh base sizes of 75%, 100%, 125%, 150% and 200% relative to the full scale base size given in Table 2. For each of the above simulations the near wall hexahedral mesh cells were kept constant to ensure suitable y+ values for each simulation.

2.11.2 Validation

2.11.2.1 Resistance

Two categories of model test data were collected by Offshore Research Ltd. for the *RAstar 3500* hull, *Irshad*: resistance data and escort data. The escort data was determined to be unsuitable for validation purposes as the model included thrusters with unknown geometry. The comparison of experimental to CFD results for the *RAstar 3500* hull from

was conducted solely for two sets of resistance data. One set of resistance data was for the bare hull while the other included both the hull and the skeg. The model and CFD tests were carried out at a model scale of 1:23.72 at speeds listed in Table 6. The properties and dimensions of the model used are listed in Table 7.

Table 6: List of Resistance Simulations and Speeds

No.	Speed (m/s)	Full Scale Equivalent Speed (knots)
1	0.131	6.03
2	0.174	8.00
3	0.216	9.97
4	0.238	10.96
5	0.259	11.95
6	0.281	12.94
7	0.302	13.93
8	0.324	14.91

Table 7: Resistance Validation Study Properties

Property	Units	Model	Ship
Scale		1:23.72	1:1
Length Overall	m	1.48	35.0
Length Waterline	m	1.39	33.0
Beam Overall	m	0.57	13.5
Beam Waterline	m	0.51	12.1
Draught	m	0.17	4.04
Midsection Area	m^2	0.07	39.4
Displacement	kg	74.71	997,000
Fluid Density	kg/m^3	997.6	1025
Fluid Viscosity	Pa-s	$8.887 * 10^{-4}$	$1.21 * 10^{-3}$

2.11.2.2 Escort

Since the escort data from the Irshad model tests was considered to be unsuitable for validation purposes, escort data from another set of tests was used to validate the CFD methodology outlined in this study. David Molyneux conducted a series of indirect escort tests at the Institute for Marine Dynamics (IMD) in St. John's, Newfoundland (Molyneux and Earle 2001). The model used was of the Voith Tractor Escort Tug, *Ajax*, and was designed by Robert Allan Ltd. Molyneux conducted escort model tests on the *Ajax* hull form with three different skeg geometries: IMD-523A, IMD-523B and IMD-523C. The tests were conducted by attaching the model to a carriage in a towing tank at various fixed yaw angles and recording the resultant hydrodynamic lift and drag forces generated by the hull. For each test, the model was free to heave and roll. The model included a skeg and Voith propeller guard. The Voith propulsion system was not included in the tests in order to determine the basic hydrodynamic escort performance of the hull and skeg over a range of yaw angles. Figure 2.11 shows escort model testing at a high yaw angle.

Figure 2.11: Example of Escort Model Tests (Molyneux and Bose 2007)

The escort CFD validation study was conducted by generating a 3D model of the Ajax hull, skeg and Voith propeller guard and calculating the lift and drag values at the yaw angles used in the model test study. The results found from CFD were then compared

against those measured in the model tests. In the CFD simulations, the model was free to heave but was set at a fixed roll angle. Since the experimental data collected in (Molyneux and Earle 2001) did not include the resulting roll angle, an estimated roll angle was used. This simplification will add a degree of error to the validation comparison, but it was assumed that generated lift and drag forces would not change significantly over small changes in roll angle. The 3D model of the Ajax used in the CFD simulations is shown in Figure 2.12.

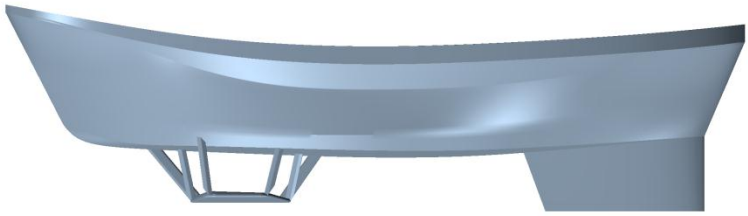

Figure 2.12: Ajax Hull Form IMD-523C

The particulars of the model used in the experimental and CFD studies are given in Table 8.

Table 8: Escort Validation Study Properties

Property	**Units**	**Model**	**Ship**
Scale		1:18	1:1
Length Overall	m	2.22	40.0
Length Waterline	m	2.12	38.2
Beam Waterline	m	0.789	14.2
Draught	m	0.211	3.80
Displacement	kg	219	1,276,000
Fluid Density	kg/m^3	999.9	1025
Fluid Viscosity	Pa-s	$1.62 * 10^{-6}$	$1.19 * 10^{-6}$

Table 9: List of Escort Simulations, Yaw and Heel Angles for 8 knots

No.	Yaw Angle (deg)	Assumed Heel Angle (deg)
1	1.4	0
2	11.4	2
3	16.5	2.5
4	21.5	3
5	26.5	4
6	31.5	5
7	36.5	6
8	41.6	7
9	46.6	10

2.11.3 Escort Analysis

The primary simulations conducted for this study involved analyzing the hydrodynamic forces and moments on the escort tug through yaw angles ranging from 0 to 90 degrees at 10 degree increments. This was done to determine a wide spectrum of hydrodynamic forces experienced by the tug through typical indirect escort operations. The analysis was done at both 1:10 model scale and full scale in order to both quantify the fluid induced forces and moments as well as the scaling effects associated with studies conducted at two significantly different Reynolds Numbers. Table 10 lists the escort simulations conducted for both full scale and model scale. Each study was conducted for a full scale speed of 8 knots. The corresponding model scale speed for the equivalent Froude Number was found from equation (3).

Table 10: List of Escort Simulations

No.	Yaw Angle (deg)	Heel Angle (deg)
1	0	0.0
2	10	3.4
3	20	6.9
4	30	9.4
5	40	9.9
6	45	9.5
7	50	9.2
8	60	7.2
9	70	6.8
10	80	5.8
11	90	4.8

Since the speed and dimensions of the vessel remained consistent for each simulation, the Froude number and Reynolds number also remained constant for each simulation. The Froude and Reynolds numbers are shown in Table 11.

Table 11: Froude and Reynolds Numbers

Froude Number	Full Scale Reynolds Number	Model Scale Reynolds Number
0.23	1.15×10^8	3.64×10^6

The model particulars used in the escort analysis for both the full and model scales are shown in Table 12.

Table 12: Ship and Model Particulars

Property	Units	Full Scale Values	Model Scale Values
Length Overall	m	35.0	3.5
Length Waterline	m	33.0	3.3
Beam Overall	m	13.5	1.35
Beam Waterline	m	12.1	1.21
Draught	m	4.03	0.403
Midsection Area	m^2	39.4	0.394
Displacement	kg	997,000	997
Model Scale		1:1	1:10
Water Density	kg/m^3	997.56 kg/m^3	997.56 kg/m^3
Water Dynamic Viscosity	Pa-s	$8.887 * 10^{-4}$	$8.887 * 10^{-4}$

The thrust and towpoint positions relative to the tug center of gravity were used in the escort force calculation and are shown in the following table. The distances are given according to the coordinate system shown in Figure 2.3. As such, negative longitudinal values imply the position is aft of the C.G. and positive longitudinal values imply the position is forward of the C.G.

Table 13: Thrust and Towpoint Positions for Full and Model Scale Escort Force Analysis

Property	Symbol	Units	Full Scale Values	Model Scale Values
Longitudinal Towpoint Position	LTS_{CG}	m	11.3	1.13
Transverse Towpoint Position	TTS_{CG}	m	0.00	0.00
Vertical Towpoint Position	VTS_{CG}	m	3.18	0.318
Longitudinal Thrust Position	LZD_{CG}	m	-12.9	-1.29
Transverse Thrust Position	TZD_{CG}	m	0.00	0.00
Vertical Thrust Position	VZD_{CG}	m	-4.78	-0.478

Chapter 3

Discussion of Results

The salient results of the escort performance prediction CFD simulations are presented in the following section. The results are presented in three categories:

1. Grid studies;
2. Validation; and,
3. Escort performance.

A domain independence study was not conducted. This was due both to the limited computational resources available and the fact that the chosen domain size met or exceeded the recommended dimensions for a CFD resistance study (CD-adapco 2011).

3.1 Grid Studies

Grid independence studies were completed both at 1:10 model scale and full scale in order to quantify the influence of the mesh density on the CFD escort force results. All meshing parameters in the simulation are based off of a single mesh base size. By changing the mesh base size the entire simulation mesh density is influenced. As such, the grid studies were conducted by varying the mesh base size to achieve denser or coarser meshes.

3.1.1 Model Scale – Resistance

The model scale grid studies were completed at a yaw angle of 0° with varying mesh base sizes and the same overall mesh distribution and prism layer settings. The mesh base sizes used as well as the calculated forces are shown in Table 14. A plan view of the volumes meshes is shown in Figure 3.1.

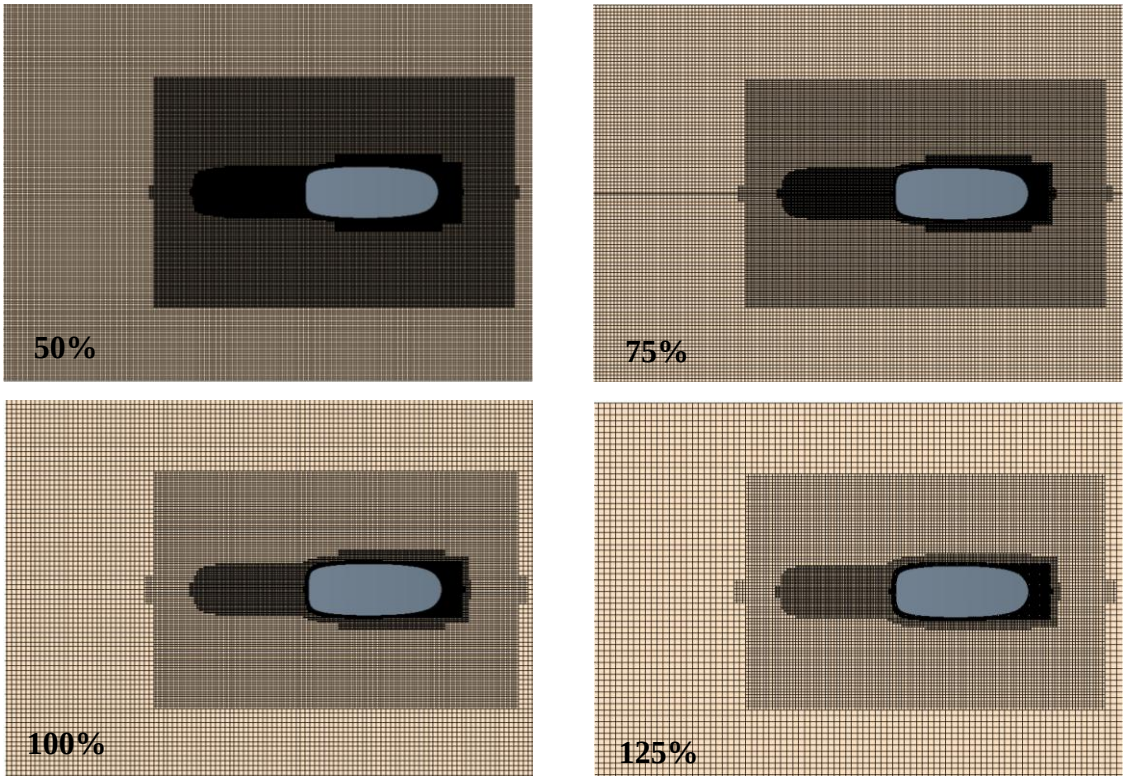

Figure 3.1: Plan View of Model Scale Resistance Grid Study

Table 14: Model Scale Resistance Grid Study Results

No.	Base Size		Drag (N)		
	(%)	(m)	Frictional	Residuary	Total
1	50	0.250	17.0	11.8	28.7
2	75	0.375	17.0	12.1	29.2
3	100	0.500	17.0	12.6	29.5
4	125	0.625	16.8	12.9	29.7

The base size of 100% represents the mesh size used for all model scale yaw angles. The % differences were determined by dividing the force by the equivalent force at a mesh base size of 100% as shown below:

$$\%\, Difference = \frac{F}{F_{100\%}} - 100\% \quad \textbf{(29)}$$

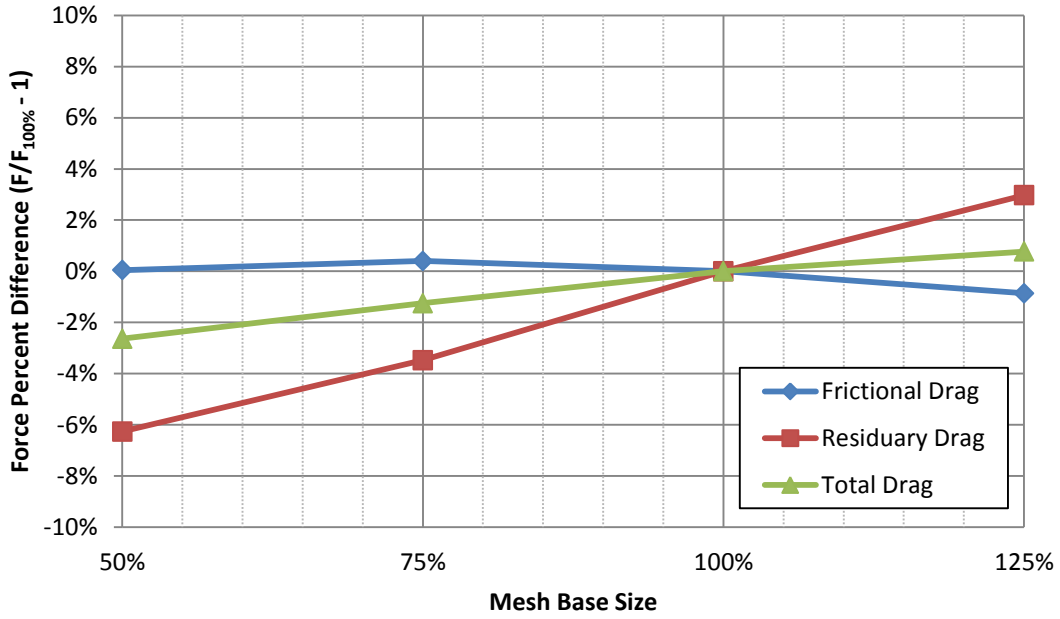

Figure 3.2: Model Scale Grid Study Force Percent Differences

It is evident from Figure 3.2 that as the mesh density increases from a base size of 100% down to 50%, the shear drag remains the same but the residuary drag decreases linearly such that it is 6.3% lower at a mesh base size of 50%. Since the frictional drag remains constant, the total calculated drag only decreases by 2.6% at a mesh base size of 50%. Therefore, as a mesh base size of 50% (0.25m) was impractical for the majority of simulations due to the long solve time and the total drag results were found to be within 3%, the selected base size of 0.5m was considered adequate for the model scale escort simulations.

3.1.2 Full Scale – Escort

A full scale grid study was completed for an escort condition at a yaw angle of 40° in order to determine the sensitivity of the lift and drag forces to mesh density. The mesh sizes were relative to the primary base size of 5.0 meters and ranged from a relative size of 75% to 200%. The meshes used are shown in Figure 3.3 and the results of the full scale, indirect grid study are shown in Table 15 and Figure 3.4.

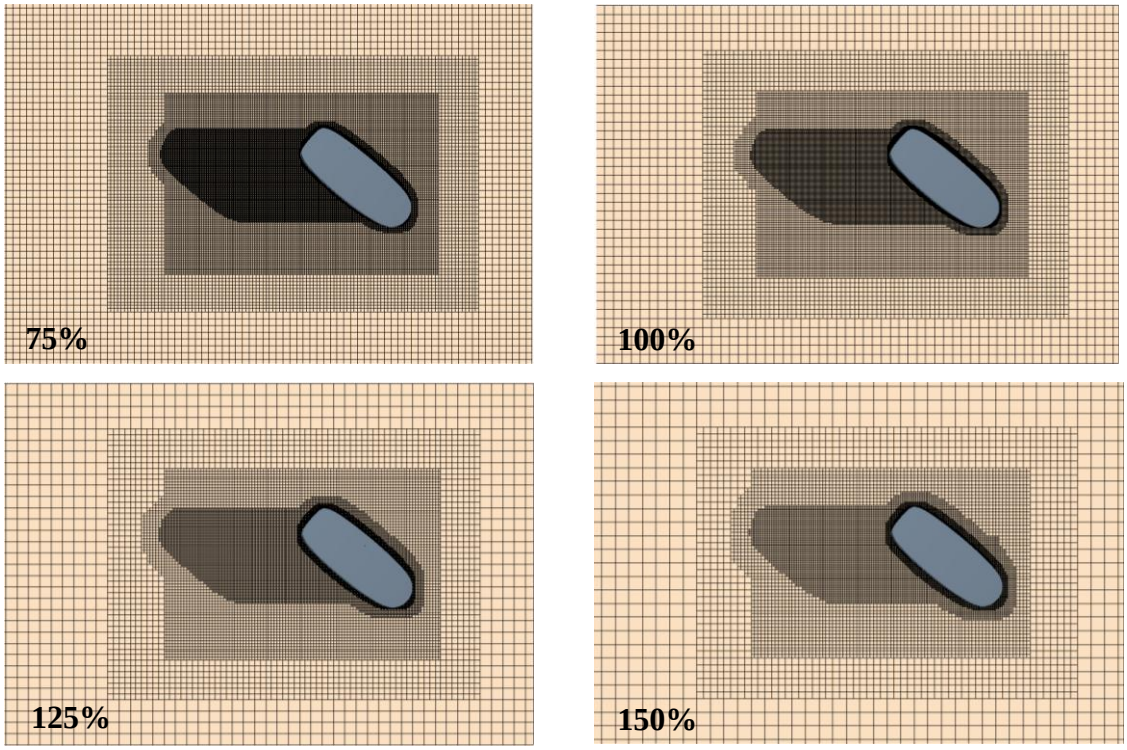

Figure 3.3: Plan View of Full Scale Escort Grid Study

Table 15: Full Scale Escort Grid Study Results[2]

No.	Base Size		Drag (kN)			Lift (kN)
	(%)	(m)	Frictional	Residuary	Total	
1	75	3.75	-8.97	-685	-694	-911
2	100	5.00	-8.63	-686	-694	-902
3	125	6.25	-8.54	-673	-681	-893
4	150	7.50	-8.63	-669	-677	-889
5	200	10.0	-8.34	-673	-682	-879

Since the vessel is at a high angle of attack the residuary lift and drag forces are much higher than the frictional forces. Because of this, only the total drag, which is nearly

[2] Sign convention of lift and drag forces is in accordance with the coordinate system shown in Figure 2.3

equivalent to the residuary drag, and the lift forces are plotted. All values are given according to the sign convention defined in Figure 2.3.

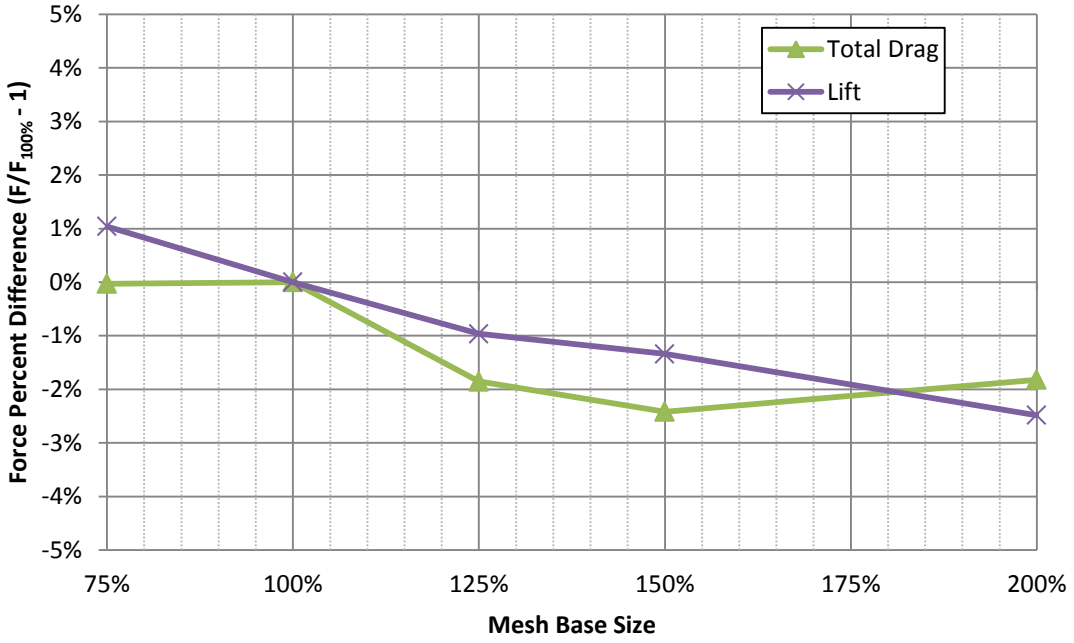

Figure 3.4: Full Scale Escort Grid Study

It is evident from the above figure that the total drag and lift forces do not change significantly in the range of mesh densities used. The maximum drag difference occurs at a mesh size of 150% and is 2.4% lower than the values found with a mesh size of 100%. Even though the results do not show a significant sensitivity to the range of mesh densities from 3.75 to 10 meters, a base size of 5 meters was chosen to be conservative.

3.2 Validation

3.2.1 Resistance

Validation is an essential part of any CFD project. When attempting to simulate a situation where existing CFD documentation is rare, the CFD user must be able to compare CFD and experimental results. This comparison provides the user with a reality check to ensure some of the core assumptions, such as the choice of turbulence model, mesh density and time-step, are justified.

In July of 2004, several towing tank model test were conducted on the Irshad model at the UBC towing tank by Offshore Research Ltd. Two hull configurations were used to collect resistance data at a range of speeds:

1. Bare-hull resistance data; and,
2. Hull and skeg resistance data.

The speeds used for the model test analysis are listed in Table 6. The CFD and model test results are shown in Figure 3.5 and Figure 3.6.

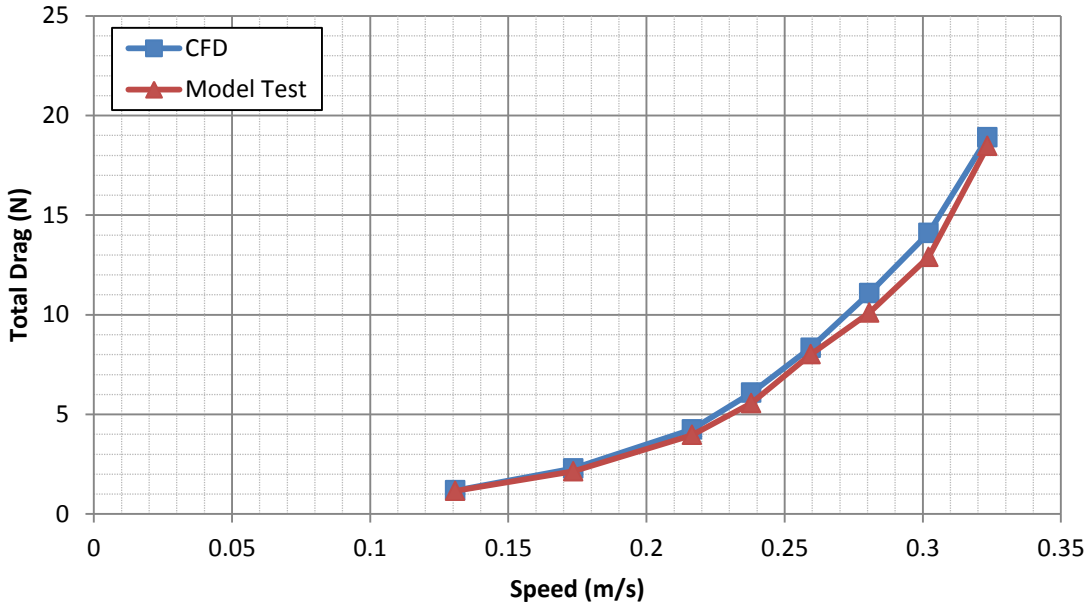

Figure 3.5: Bare Hull Resistance Curve

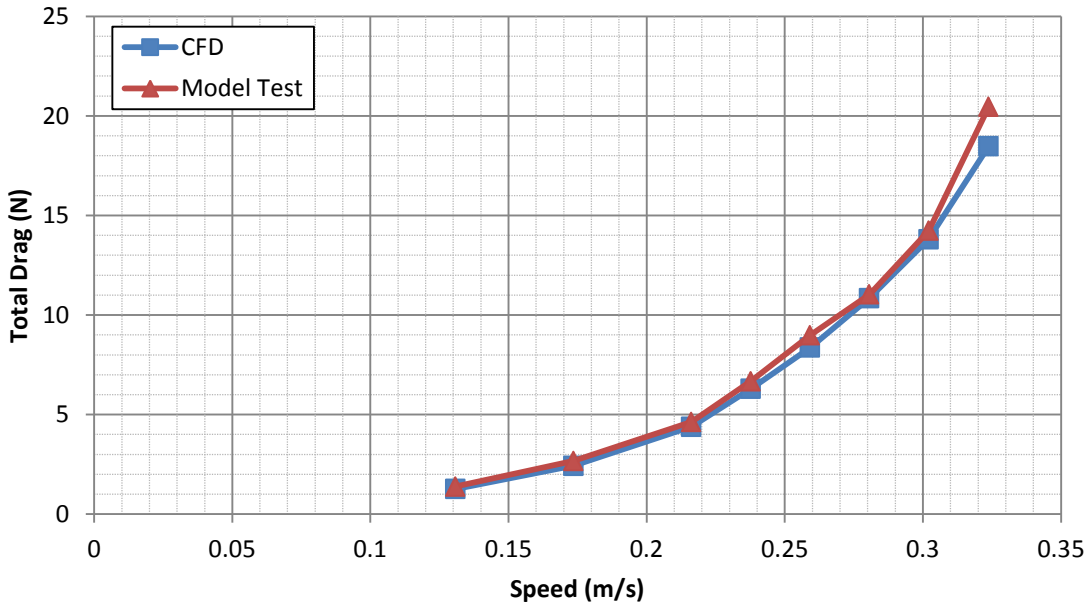

Figure 3.6: Hull with Skeg Resistance Curve

The maximum percent different between the model and CFD results for the bare hull and hull with skeg conditions was 9.25% at 0.281 m/s and 10.16% at 0.324 m/s respectively. The average percent difference was 6.04% for the bare hull case and 6.43% for the hull with skeg case.

The comparisons given in Figure 3.5 and Figure 3.6 show that independent CFD and experimental studies of the same model at identical speeds produces similar results.

3.2.2 Escort

The CFD escort validation study was conducted according to the methodology outlined in Section 2.11.2.2 in order to replicate the escort model tests conducted by David Molyneux at the IMD. For each simulation the yaw and heel angles were set and the model fixed in all directions except vertical translation (heave). The absolute values of the experimental and CFD hydrodynamic lift and drag forces are compared in Figure 3.7.

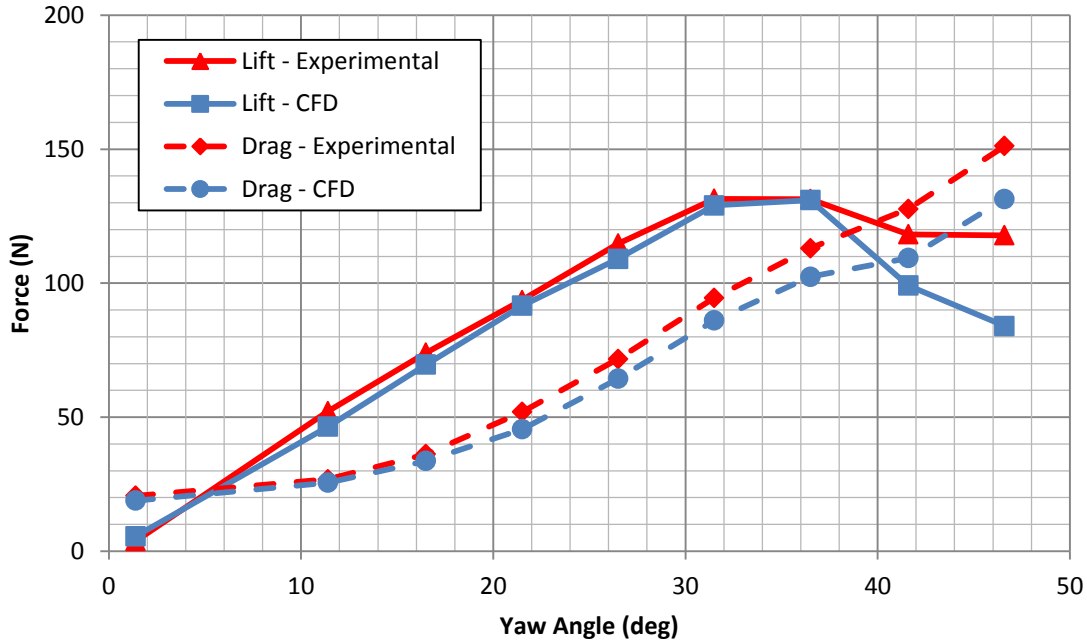

Figure 3.7: CFD Validation against Experimental Escort Data of the Ajax Hull Form

The complete table of experimental data collected in the escort model tests of the *Ajax* hull form is given in Appendix B. From Figure 3.7 it is evident that the lift and drag forces determined in CFD closely match those found in model tests. Both predict that stall will occur at a yaw angle of approximately 37 degrees, as evident by the sudden drop in lift. However, after stall occurs, the lift found from CFD drops more rapidly than the lift found in the model tests. This under prediction of lift in CFD may be a result of the k-ε turbulence model which is known to struggle in the accurate calculation of highly separated flows (Wilcox 2006).

The trend of the hydrodynamic drag determined in CFD closely matches the experimental values. However, as the yaw angle increases, the drag found in CFD appears to under predict the actual drag. The difference in drag values appears to increase slowly with yaw angle until the gap is increased further still past the point of flow separation at 37 degrees. Although the difference in the drag values increases suddenly after stall, the CFD simulation appears to pick up the sudden decrease in lift-induced-drag as is evident by the inflection point in the drag curve at a yaw angle of 42 degrees. This inflection point is also evident in the experimental results, although to a lesser extent.

In order to further explore the reasons for the difference in lift and drag forces between the CFD and experimental models, further work should be conducted in the area of turbulence model and mesh refinement at yaw angles around the point of stall. Since the results presented in Figure 3.7 indicate a favourable correlation between the CFD and experimental escort results, it is believed that an accurate prediction of escort forces can be achieved with the method presented in this paper.

3.3 Escort Performance

To analyze the indirect escort performance of the escort tug, *Irshad*, full scale CFD simulations were conducted for yaw angles ranging from 0° to 90°. Additionally, 1:10 model scale simulations were conducted for the same yaw angles to quantify the scaling effects on escort forces. A plan view of the wake for the simulations at a yaw angle of 40° for both full and model scales is shown in Figure 3.8.

The results in the following sections are presented as a comparison between the model and full scale simulations and are grouped into three categories:

1. Lift and drag coefficients;
2. Flow separation and streamlines; and,
3. Pressure distribution.

In order to assess the escort performance of the *Irshad* from the full and model scale simulation, the final section outlines how to calculate escort forces from the hydrodynamic forces and moments calculated in CFD.

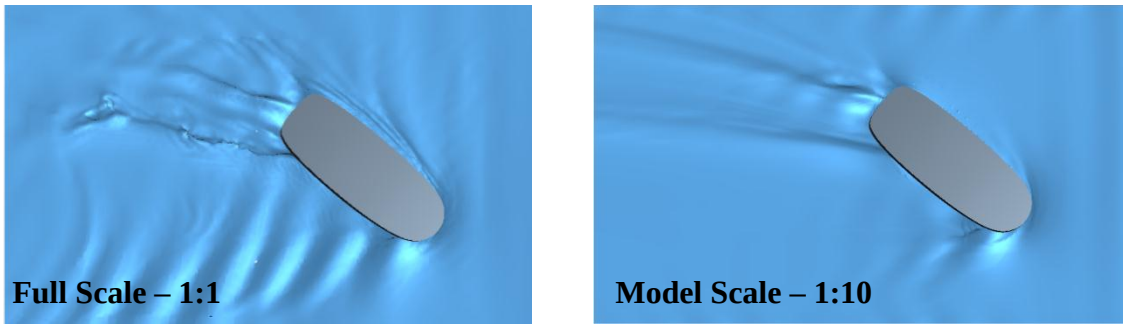

Figure 3.8: Full and Model Scale 40° Yaw Wake Plan View Comparison

3.3.1 Lift and Drag Coefficients

The lift and drag coefficients are defined as (White 2003):

$$C_D = \frac{H_X}{\frac{1}{2}\rho V^2 A} \quad \textbf{(30)}$$

$$C_L = \frac{H_Y}{\frac{1}{2}\rho V^2 A} \quad \textbf{(31)}$$

Where:

	C_D	Drag Coefficient
	C_L	Lift Coefficient
	H_X	Drag Force
	H_Y	Lift Force
	ρ	Fluid Density
	V	Fluid Free Stream Velocity
	A	Characteristic Area

With H_X and H_Y defined according to the sign convention given in Figure 2.3. The characteristic area can be determined two different ways. Conventionally, the wetted area is used for surface ships, the frontal area for thick, stubby bodies such as cylinders, cars or torpedoes and the planform area for wings and hydrofoils (White 2003). However, since the escort tug is moving through the water at a non-zero angle of attack, the tug resistance is composed primarily of pressure, or form, drag and behaves more like a blunt body rather than a typical surface ship where frictional drag has a dominant role. Figure 3.9 shows the plot of lift coefficient vs. yaw angle for both model and full scale cases determined using the wetted and frontal areas and Figure 3.10 shows the plotted drag coefficients.

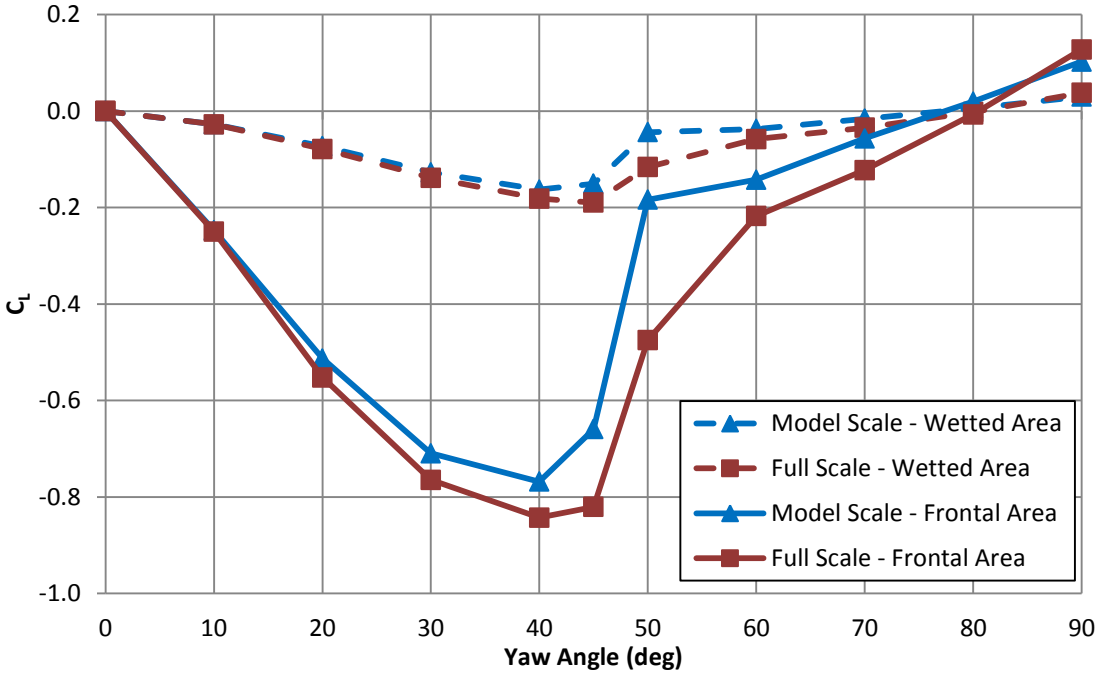

Figure 3.9: Lift coefficients for model and full scales using both wetted and frontal areas as a function of tug yaw angle

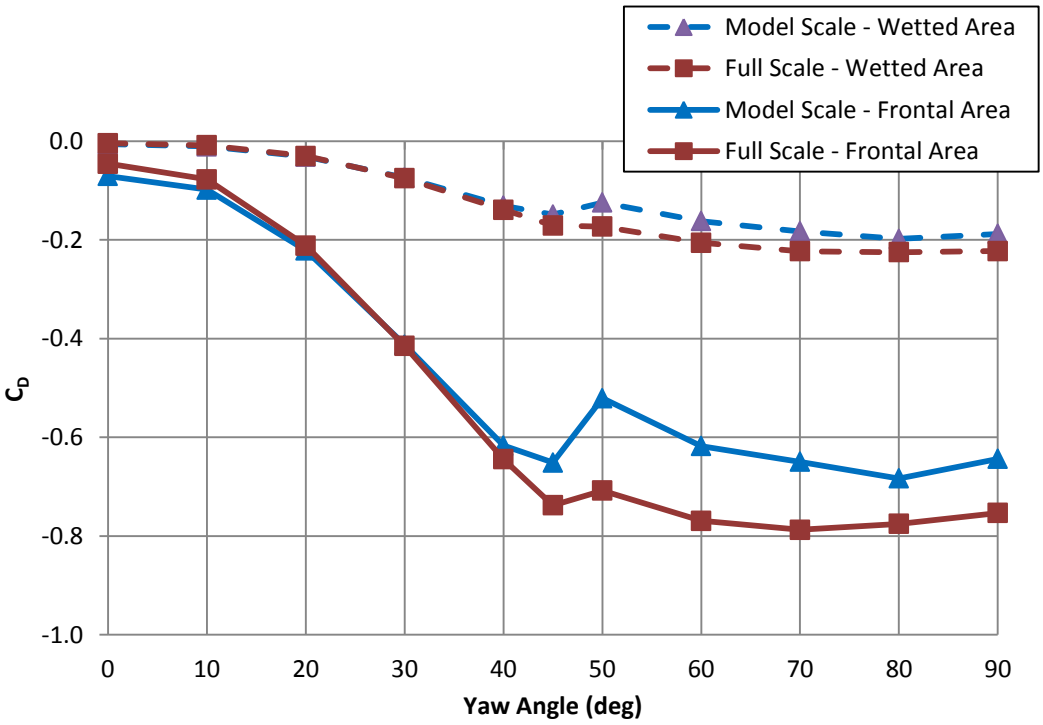

Figure 3.10: Drag coefficients for model and full scales using both wetted and frontal areas as a function of tug yaw angle

The trends of the lift and drag coefficient plots shown above are similar when using either the frontal or wetted area. The main difference between the two coefficients is the curve generated by using the wetted area ranges from 0 to -0.2 while the curve using the frontal area ranges from 0.0 to -0.8. As such, either coefficient would be suitable in non-dimensional analysis of escort forces.

It is evident from Figure 3.9 that the lift forces calculated for the model and full scale simulations are consistent up to a yaw angle of 10°, and begin to diverge at an angle of 20°. This difference increases as the yaw angle increases. The difference increases even further when the lift force drops off significantly at a yaw angle of 45 degrees for model scale and at 50 degrees for full scale. The significant decrease in lift forces is due to flow separation on the low pressure side of the hull, resulting in the hull stalling, similar to what occurs with an airfoil at high angles of attack. The discrepancy between the model and full scale simulations from yaw angles of 20° to 80° is believed to be a result of the large difference in Reynolds number which influences the degree and position in which flow separation occurs.

The drag values, shown in Figure 3.10, are different between scales for yaw angles of 0 to 10 degrees. From 20 to 40 degrees the drag coefficients are within 5%. At 45 degrees the model scale drag is 12% less than at full scale. At both model and full scale, the drag decreases at 50 degrees before increasing. This brief decrease in drag can be attributed to the loss of lift-induced-drag as it corresponds to the hull stall position. The drag increases again at angles higher than 50 degrees as the frontal area seen by the flow increases.

It can be concluded from both Figure 3.9 and Figure 3.10 that the lift forces in the model and full scales are comparable for largely attached flow regimes but differ significantly once flow separation occurs.

The complete list of calculated forces, areas and moments is given in Appendix C.

3.3.2 Flow Separation and Streamlines

To further explore the scaling effects on escort forces, the wall shear stress and flow patterns were analyzed for both cases.

In order to confirm that the difference in model and full scale escort forces was, in-part, due to differing flow separation, the wall shear stress on the hull of both cases was compared. The figures below display a comparison of wall shear stress for both model and full scales at yaw angles from 30° to 60°, as this is the range of largest discrepancy between lift and drag forces. Because of the coordinate system defined in Figure 2.3, with the flow moving in the negative X-direction, a negative wall shear stress indicates attached flow and greater than zero wall shear stress indicates fully separated flow. The fully separated regions are indicated as solid blue enclosed by a black outline.

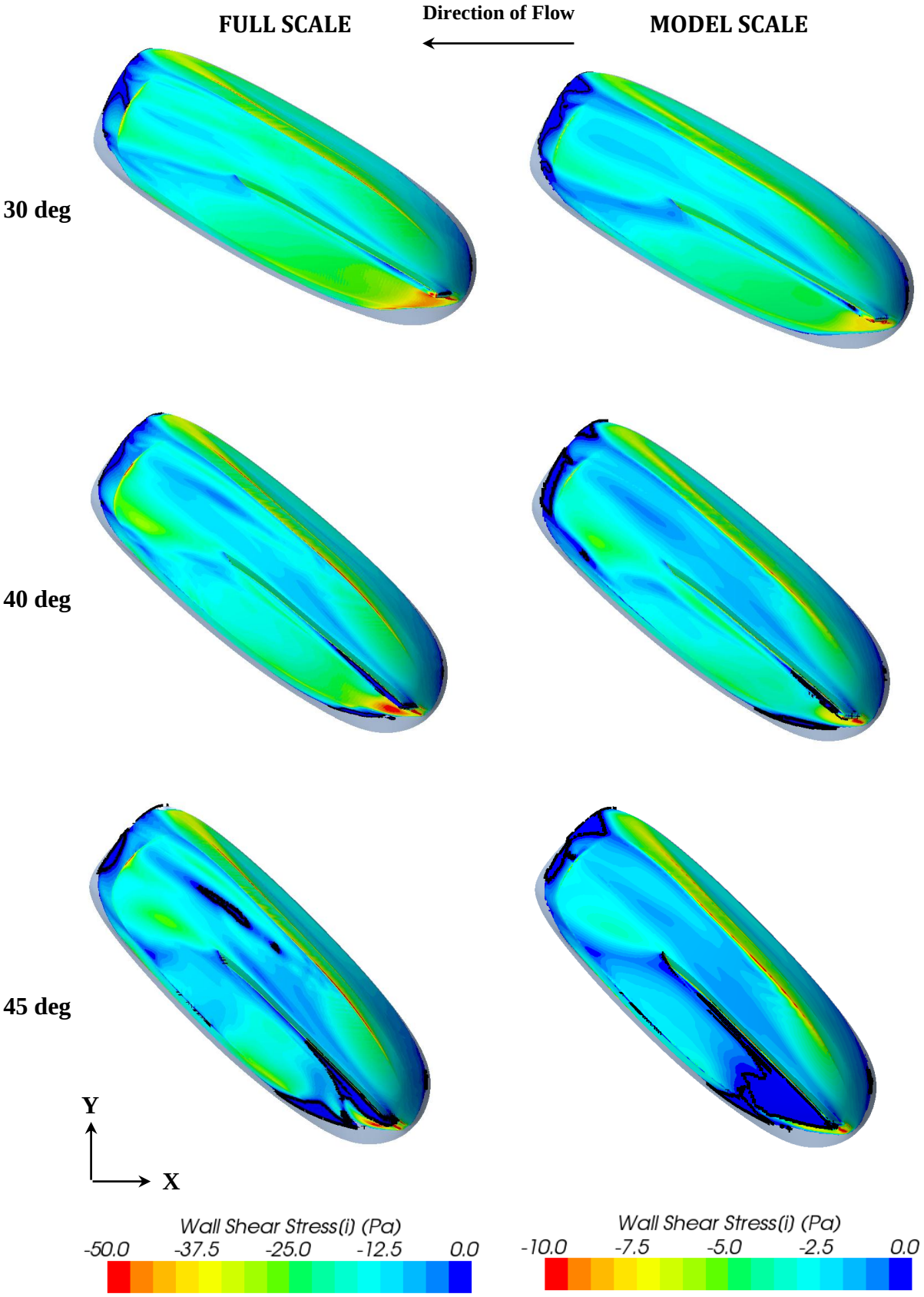
FULL SCALE
Direction of Flow
MODEL SCALE
30 deg
40 deg
45 deg
Y
X
Wall Shear Stress(i) (Pa)
-50.0
-37.5
-25.0
-12.5
0.0
Wall Shear Stress(i) (Pa)
-10.0
-7.5
-5.0
-2.5
0.0

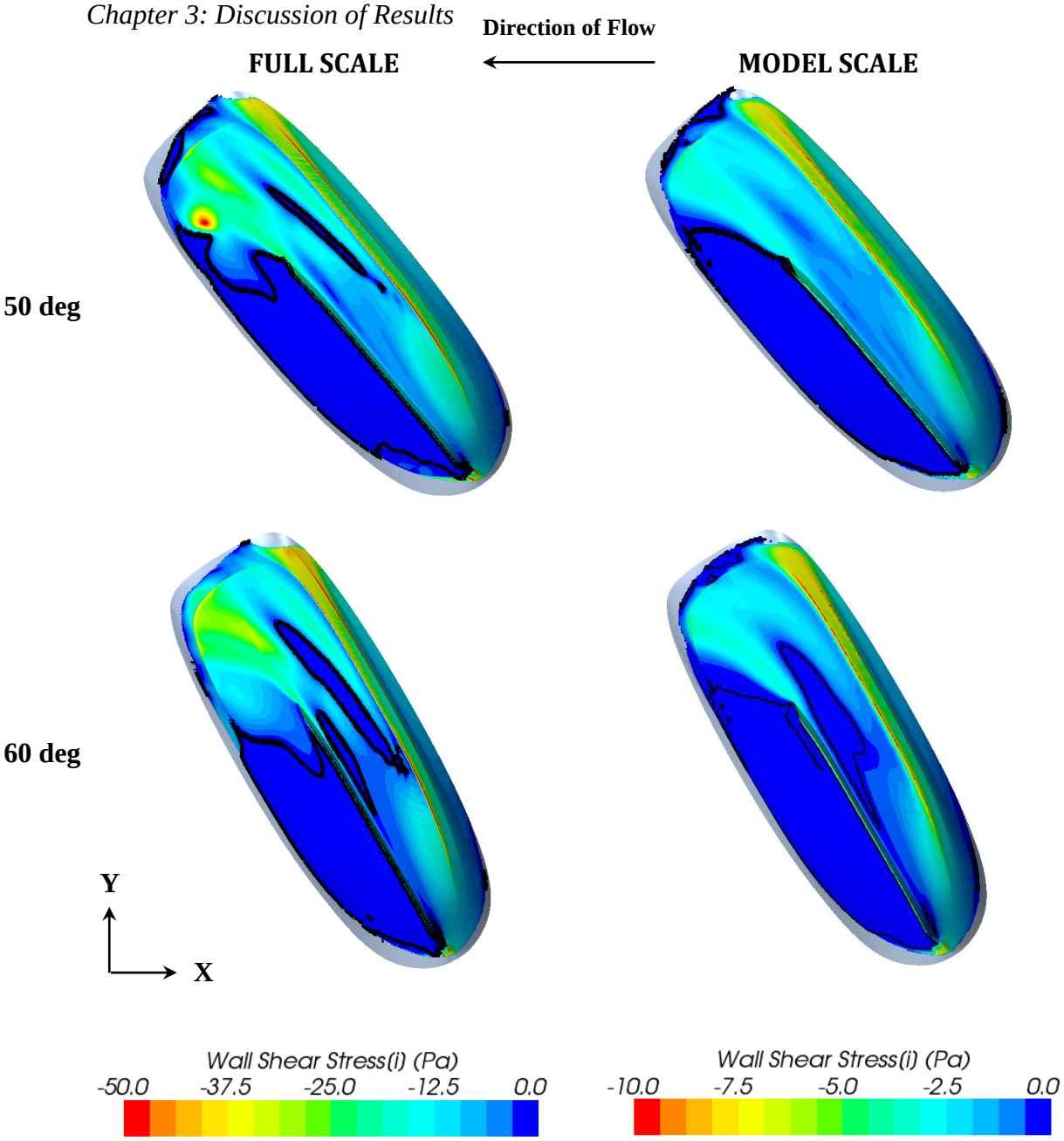

Figure 3.11: Wall Shear Stress and Flow Separation Comparison

The above figures show that flow separation begins to occur at both scales at a yaw angle of 40 degrees. At 45 degrees the flow remains largely attached but with the separation area increasing in size. Additionally, more significant flow separation is evident at model scale than full scale which is in agreement with the force coefficient results. At both scales, the hull is fully stalled in the region behind the skeg at a yaw angle of 50 degrees. This corresponds with the rapid decrease in lift force observed in Figure 3.9.

The flow streamlines, with the colour representing flow velocity, were also plotted to further visualize the physical fluid conditions associated with indirect escort hydrodynamic forces. The plots were generated for the same range of yaw angles, 30 to 60 degrees, as used in the wall shear stress diagrams.

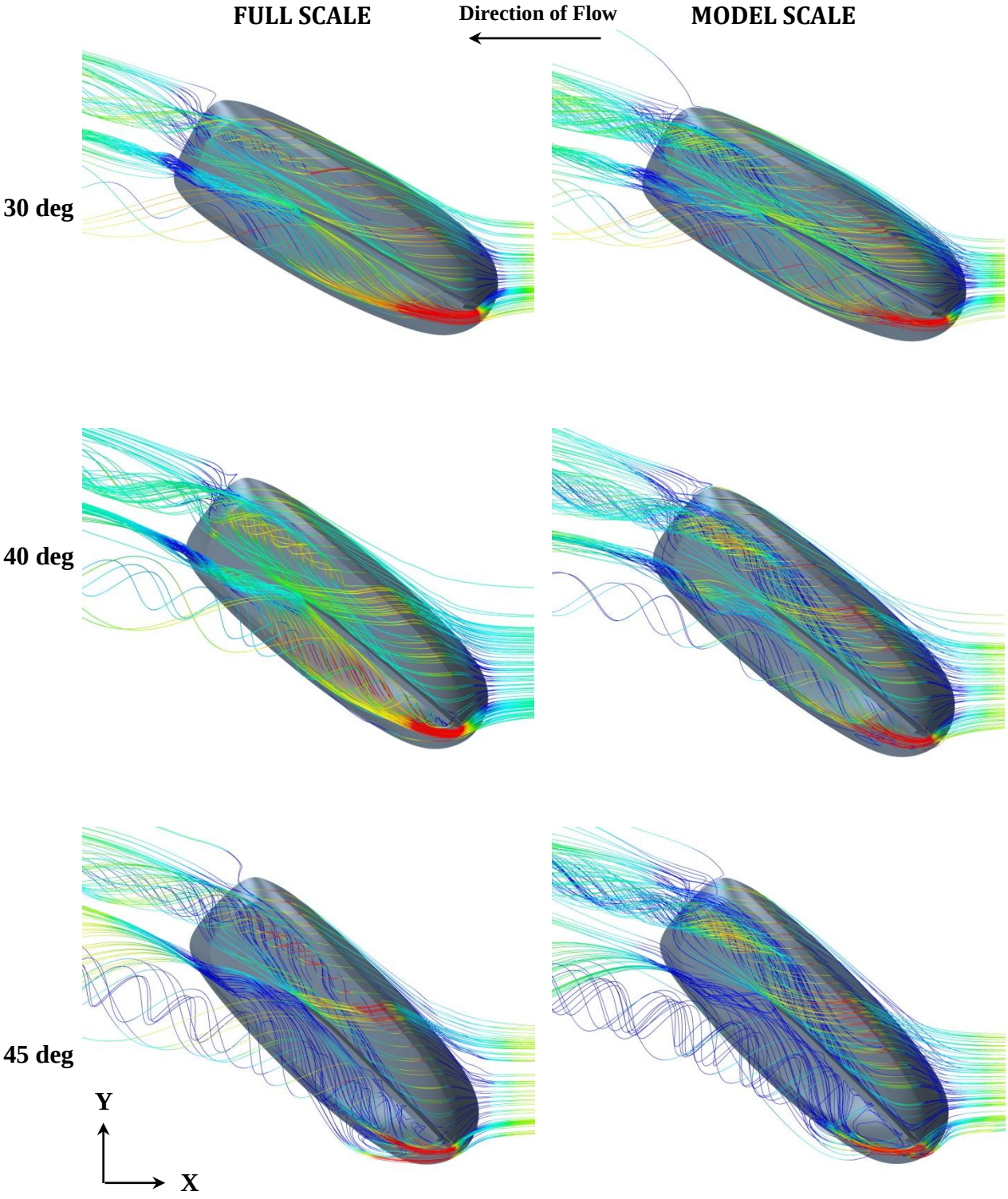

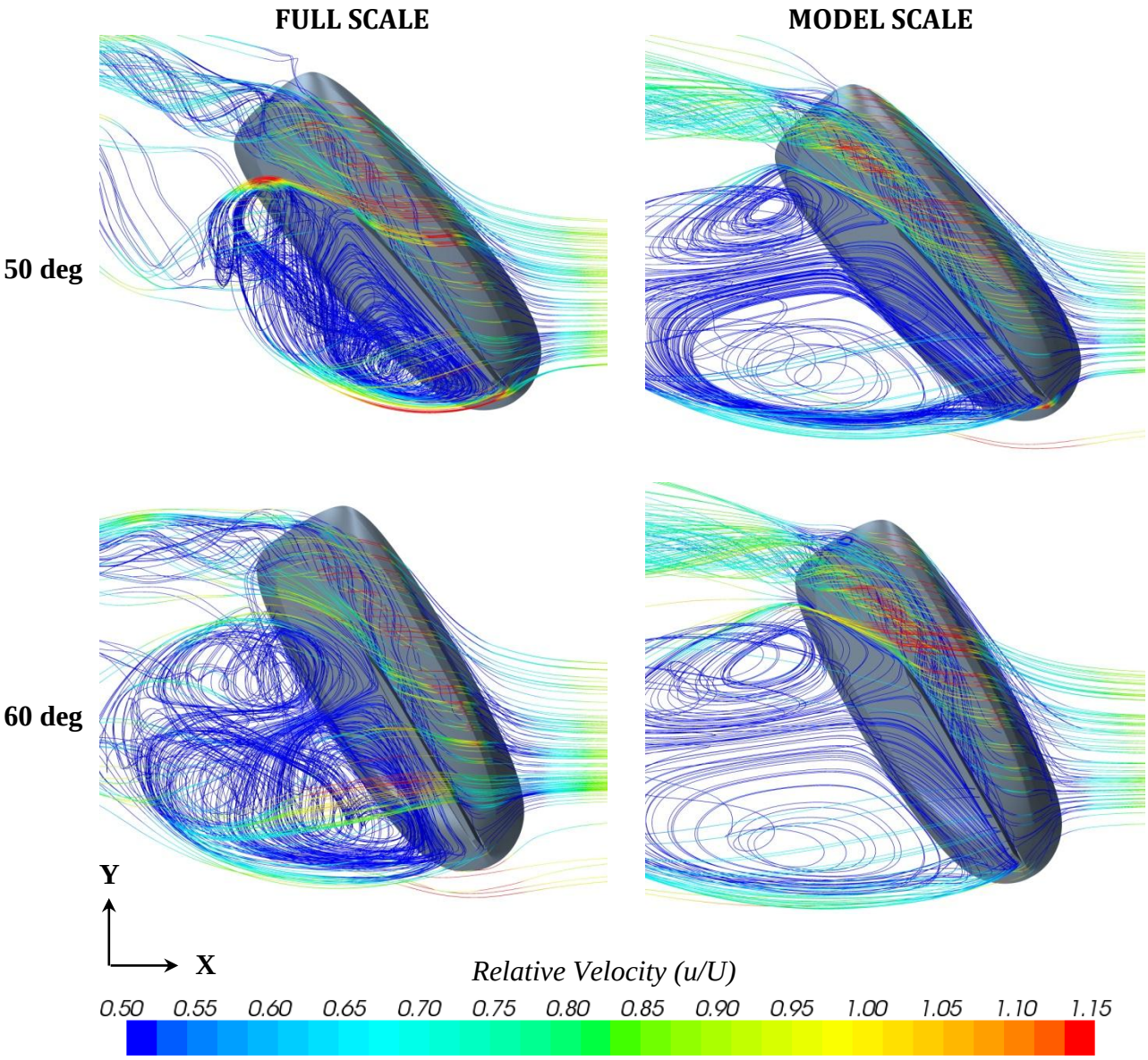

Figure 3.12: Flow Streamline Comparison

Using the flow streamlines, the progress of separation, beginning at 40 degrees and becoming fully separated at 50 degrees, was observed. At 30 and 40 degrees, the flow was similar between the model and full scale cases. Beginning at 45 degrees, the flow began to separate more significantly than at full scale. This was due to the higher Reynolds number at full scale, resulting in higher flow momentum in the boundary layer which allowed the flow to remain attached at more aggressive yaw angles. By 50 degrees

both the full and model scale cases had significant flow recirculation occurring past the skeg. In the full scale case, the flow recirculation was more chaotic and unstable whereas in the model scale case, the recirculating flow features a large and a small structured recirculation zone emanating from the fore and aft end of the skeg respectively. This structured flow separation phenomenon in the model scale case can be attributed to the high viscous effects present due to the relatively low Reynolds number.

3.3.3 Pressure Distribution

The pressure coefficient was plotted on the surface of the hull for the full and model scale cases at each yaw angle. The pressure coefficient is defined as (White 2003):

$$C_p = \frac{p - p_\infty}{\frac{1}{2}\rho U^2} \quad \textbf{(32)}$$

Where:

	C_p	Pressure Coefficient
	p	Absolute Pressure
	p_∞	Hydrostatic Pressure
	U	Free Stream Velocity
	ρ	Fluid Density

The plotted pressure coefficient for the full and model scale simulations is compared for yaw angles of 30 to 60 degrees in the figures below.

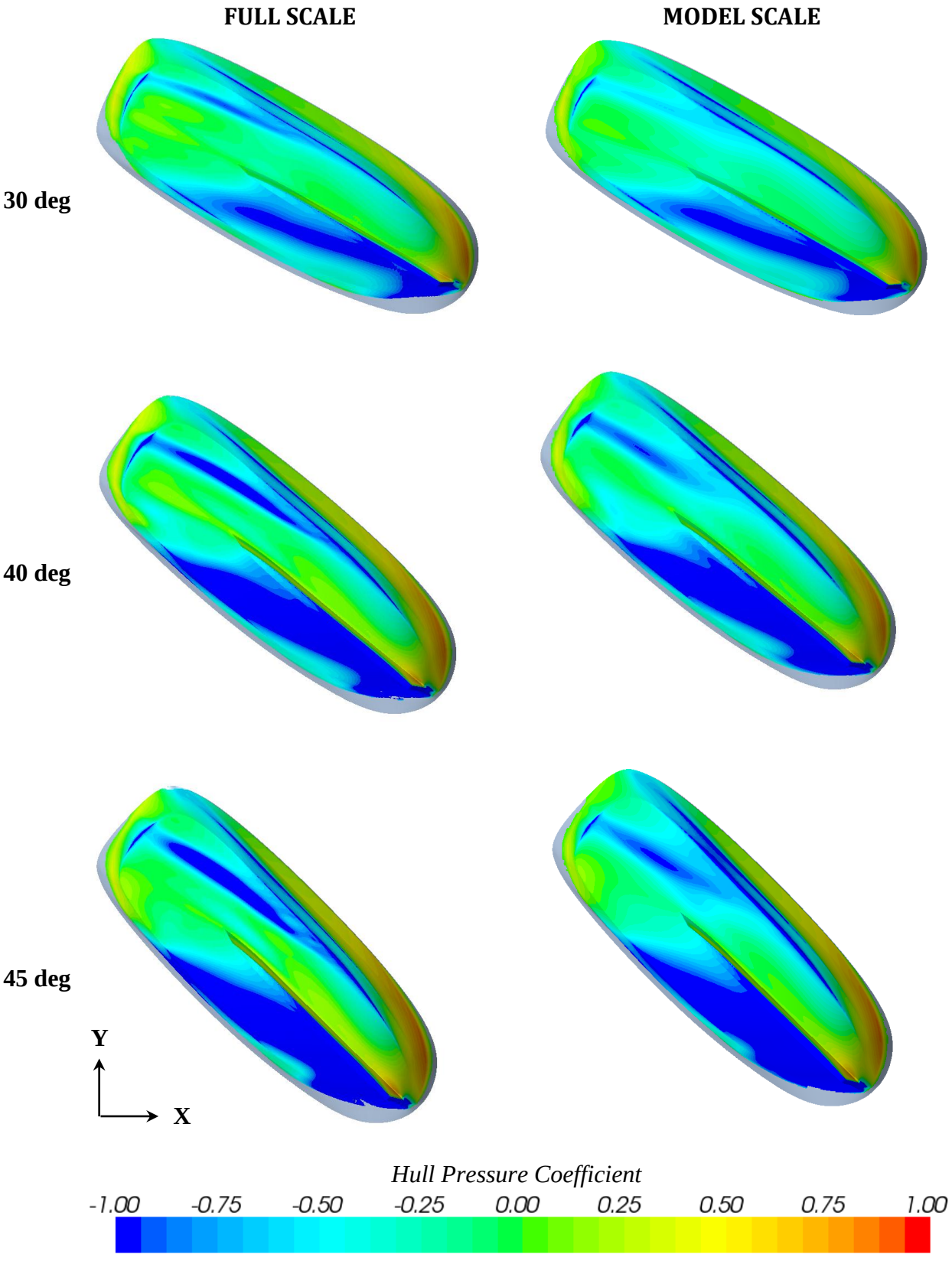
FULL SCALE
MODEL SCALE
30 deg
40 deg
45 deg
Y
X
Hull Pressure Coefficient
-1.00
-0.75
-0.50
-0.25
0.00
0.25
0.50
0.75
1.00

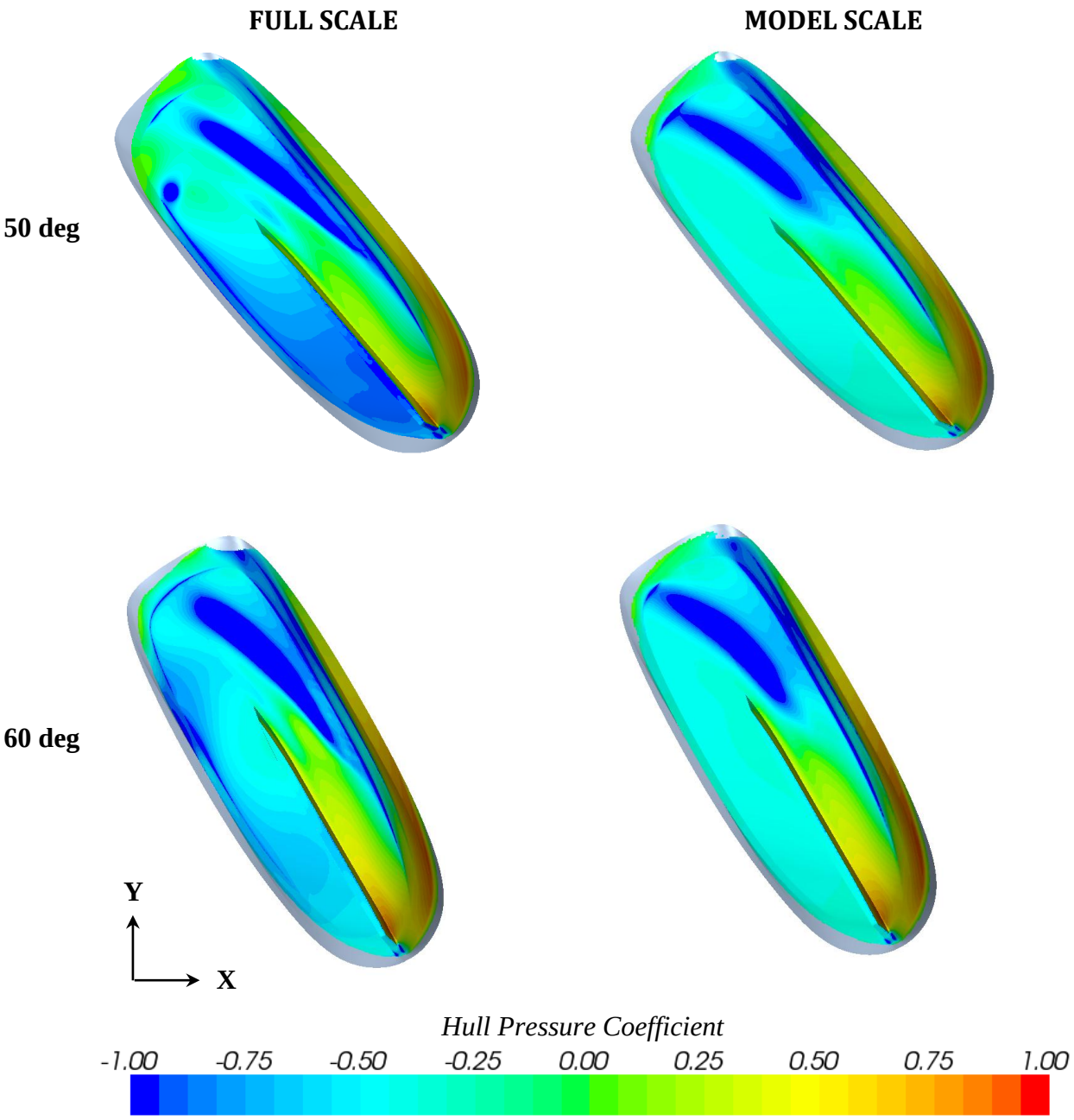

Figure 3.13: Hull Pressure Coefficient Comparison

The above figures show that the pressure distribution on the hull remained very similar between the two scales for yaw angles of 30 to 45 degrees. At 50 degrees, the pressure on the downstream side of the model scale hull increased as the flow became fully separated.

Comparatively, the pressure on the downstream side of the full scale hull remained lower at 50 degrees for the full scale case.

The lower hull pressure at higher yaw angles implies that, at full scale, the hull can achieve higher steering forces as stall occurs slightly later than at model scale. In order to quantify the potential difference in predicted escort steering forces between full and model scales, the following section outlines the calculation of escort forces from the CFD simulation hydrodynamic forces.

3.3.4 Calculation of Escort Forces

The forces and moments that contribute to a tug's escort performance are the:

1. Hull hydrodynamic lift and drag forces and yawing moment;
2. Towline force; and,
3. Thrust force.

The hull hydrodynamic forces and moments were known from CFD but the towline and thrust forces had to be calculated. By balancing the forces shown in the free-body-diagram below, the towline and thrust forces were determined.

Where:

X*:	Local X Direction
Y*:	Local Y Direction
T_T:	Transverse Towline Force
T_L:	Longitudinal Towline Force
P_T :	Transverse Thrust Force
P_L :	Longitudinal Thrust Force
H_T :	Transverse Hydrodynamic Force
H_L :	Longitudinal Hydrodynamic Force
M_{YAW}:	Hydrodynamic Yawing Moment
LZD_{CG}:	Longitudinal Distance from Thrusters to C.G.
LTS_{CG}:	Longitudinal Distance from Towing Staple to C.G.

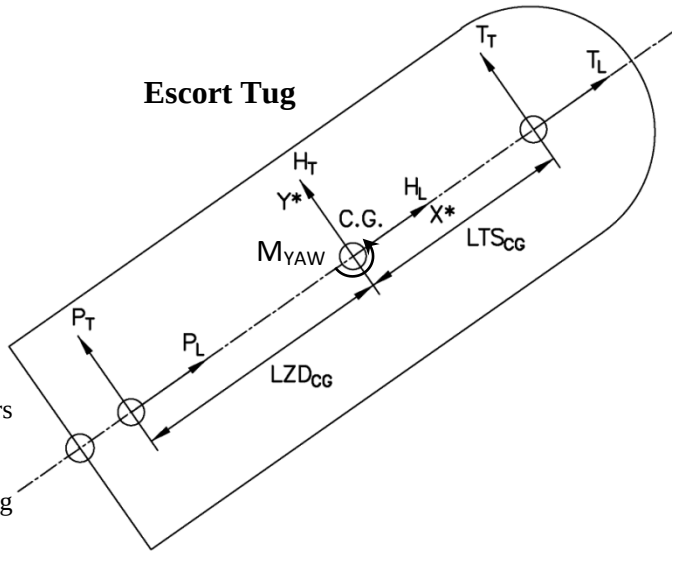

Figure 3.14: Escort Tug Free Body Diagram

The following equations were generated when the forces are balanced in the X, and Y directions. The third equation was generated by balancing the yawing moment about the ship C.G.

$$\sum F_{X^*} = 0 = P_L + H_L + T_L \quad \textbf{(33)}$$

$$\sum F_{Y^*} = 0 = P_T + H_T + T_T \quad \textbf{(34)}$$

$$\sum M_Z = 0 = M_{YAW} + T_T LTS_{CG} + P_T LZD_{CG} \quad \textbf{(35)}$$

The hydrodynamic forces and moments as well as the distance of the thrusters and towing stable to the C.G. were known from the simulations. To calculate the unknown thrust and towline forces, equations (34) and (35) were rearranged to solve for P_T and T_T, shown in the following equations.

$$T_T = -(P_T + H_T) \quad \textbf{(36)}$$

$$P_T = \frac{-(M_{YAW} + T_T LTS_{CG})}{LZD_{CG}} \quad \textbf{(37)}$$

By substituting equation (36) into (37), the required transverse thrust force was found as:

$$P_T = \frac{-M_{YAW} + H_T LTS_{CG}}{LZD_{CG} - LTS_{CG}} \quad \textbf{(38)}$$

With P_T solved, T_T was found from equation (36). The longitudinal components of thrust, towline and hydrodynamic forces were found from equation (33). The assumption was made to calculate the Pure Indirect escort forces generated by the Irshad, therefore the thrust was considered to act only in the transverse direction in the amount required to maintain the set yaw angle. As such, equation (33) simplified to:

$$\sum F_{X^*} = 0 = H_L + T_L$$

$$\therefore\ H_L = -T_L \quad \textbf{(40)}$$

Once T_T and T_L were determined, the steering and braking forces were calculated by transforming the towline force from the local escort tug coordinate system to the global coordinate system:

$$F_B = T_T \sin\theta + T_L \cos\theta \quad \textbf{(39)}$$

$$F_S = T_T \cos\theta - T_L \sin\theta \quad \textbf{(41)}$$

Where: F_B Escort Braking Force

F_S Escort Steering Force

θ Tug Yaw Angle

An escort tug butterfly diagram was created by plotting the braking force versus the steering force for each yaw condition and is shown in Figure 3.15. For completeness, the steering and braking forces were mirrored for positive and negative steering forces. The escort tug yaw angles are included next to each data point for both model and full scale conditions up to a yaw angle of 50 degrees. It is common practice to provide the escort performance in terms of tonnes rather than newtons.

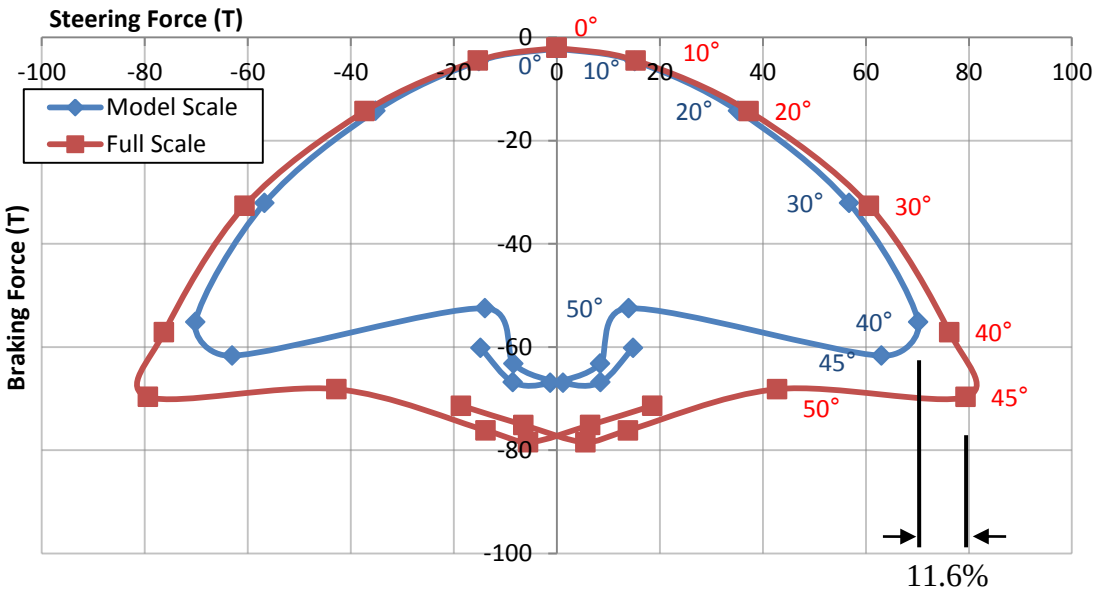

Figure 3.15: Irshad Escort Butterfly Diagram

Figure 3.15 shows good agreement between the model and full scale steering and braking forces up to a yaw angle of 40 degrees. At model scale, the hull experienced flow separation in-between 40 and 45 degrees and the lift began to decrease with the maximum steering force of 70.2 tonnes achieved at 40 degrees. At full scale, the hull experienced flow separation from 45 to 50 degrees and achieved a maximum steering force of 79.5 tonnes at 45 degrees. Therefore, the model scale escort performance was under predicted by 11.6%.

The butterfly diagram shown in Figure 3.15 was developed for the Pure Indirect mode of escort where the thrusters apply only enough transverse force to maintain the tug's yaw angle with no longitudinal thrust component. Therefore, the escort performance shown is primarily due to the hydrodynamic characteristics of the escort hull rather than the power of the thrusters. The Pure Indirect escort performance is a valuable measure by which to compare the performance of various hull geometries independent from the choice of propulsion. In practice, when assessing the absolute escort capabilities of a vessel, the Powered Indirect performance would be calculated in which the thrusters provide force in both the transverse and longitudinal directions to augment the hydrodynamic lift and drag forces generated by the tug.

For a complete escort analysis, it is important to be able to relate the thrust force vector determined from equation (36) to the azimuth angle and propeller RPM of the tug Z-Drive. This is desired in order to predict the optimal drive azimuth angle resulting in maximum steering forces as well as relate the thrust force to shaft power. With the current analysis, there is no way of knowing if the calculated thrust force exceeds the maximum thrust available at the drive. Relating the azimuth angle, drive interaction effects and resulting thrust force vector of each drive could be achieved by implementing the thrust prediction method outlined by Paul Brandner (Brandner and Renilson 1998). By using Brandner's method, the escort prediction analysis could be expanded to calculate the thrust force of each Z-drive independently. Furthermore, the determined thrust could be translated directly into drive azimuth angle as well as propeller RPM which would provide valuable information to both tug operators and designers.

Chapter 4

Conclusions

4.1 Grid Studies

Grid studies were carried out for both full and model scale simulations to establish the mesh sensitivity of the results.

The model scale grid study was conducted for a yaw angle of 0° and tested meshes with base sizes of 50%, 75%, 100% and 125% relative to chosen base size of 0.5 meters. The frictional resistance was found to remain constant over the range of meshes which was expected as the near wall prism layer thickness remained constant for each simulation. The total resistance decreased by 3% for the mesh with a base size of 50% and increased by 1% for the base size of 125%.

The full scale grid study was conducted for a yaw angle of 45° at featured mesh sizes of 75%, 100%, 125%, 150% and 200% of the chosen base size of 5.0 meters. For each mesh size the lift and drag forces were compared. When compared to the base case, the lift force was found to be 1% higher for a base size of 75% and 2.5% smaller for a base size of 200%. No difference was found between the total drag force at a base size of 75% and the base case. The total drag had a maximum deviation of 2.5% from the base case at a base size of 150%. It was therefore concluded that the chosen mesh size was grid independent.

4.2 Validation

The validation of the proposed escort CFD methodology was completed in two parts. The first part focused on the validation of a CFD resistance model using model test data of the RAstar 3500, *Irshad*, hull form. The second part involved validating the CFD

methodology used for the escort analysis by comparing escort forces calculated in CFD against model test data of the *Ajax* escort tug hull form collected by David Molyneux at IMD.

For the resistance validation, two experimental resistance cases involving hulls with and without a skeg were used for validation against the CFD model. The hull form used in both the experimental and CFD analysis was identical. The resistance results for cases with and without the skeg had an average difference of 6.04% and 6.43% respectively. For the bare hull model the maximum difference was 9.25% at a speed of 0.281 m/s and for the hull with skeg model the maximum difference was 10.16% at a speed of 0.324 m/s.

For the escort validation, a range of CFD simulations were performed for yaw angles ranging from 0 to 45 degrees and calculated lift and drag forces were compared against escort model tests of the same hull form. The CFD results for maximum lift were within 2% of the experimental values with the same stall angle of approximately 37 degrees predicted in both cases. The calculated drag force was consistently within 10% of the model test values; however, the CFD simulations increasingly under predicted drag as yaw angle increased. Once flow separation had occurred above 37 degrees the predicted lift and drag forces were significantly below the model test forces. Therefore, the proposed methodology for analyzing the performance of escort tugs in CFD can be considered valid up until the point of stall. Once stall has occurred, the error in the CFD analysis becomes significant; therefore, further work is required to refine the proposed method such that forces after the point of stall can be accurately predicted.

4.3 Escort Performance

The hydrodynamic lift and drag forces on an escort tug were calculated in CFD taking into account the resulting free surface, ship heave and detailed vessel geometry. By using the actual ship hull and skeg geometry, the predicted escort forces are more representative of the real-life escorting condition, providing increased fidelity to the proposed prediction method over current alternative methods that rely on data from

representative escort model test studies on a similar shaped vessel. As such, this method is not reliant on the existence of related model tests data, but can be applied to any novel escort tug form.

In this study, the lift and drag coefficients using the wetted and frontal areas combined with the raw lift and drag forces found in CFD, were calculated for the complete range of yaw angles and compared between model and full scale.

The lift coefficient was nearly identical between model and full scale from 0 to 10 degrees yaw and began diverge at 20 degrees. At the model scale point of maximum lift of 40 degrees yaw, the model scale lift coefficient calculated from the frontal area is 8.9% less than the full scale coefficient. At the full scale point of maximum lift of 45 degrees yaw, the model scale lift coefficient is 20% less than the full scale coefficient.

The drag coefficients between model and full scale were found to differ significantly at yaw angles of 0 to 10 degrees but were within 5% at 20 to 40 degrees. At the approximate stall position of 45 degrees, the full scale drag was 12% greater than at model scale. The loss of lift induced drag was observed at a yaw angle of 50 degrees as the drag decreased suddenly at the onset of flow separation.

The areas of flow separation and the pressure coefficient were plotted on the escort tug hull and compared between the model and full scale cases. The areas of flow separation were similar between scales for yaw angles of 40 degrees and less. At 45 degrees, flow separation was observed on the hull behind the leading quarter of the skeg; with a larger area of flow separation at model scale. At yaw angles of 60 degrees and above, the separated areas were comparable between the two scales. The hull pressure coefficient at both scales was very similar for yaw angles of 0 to 45 degrees on the downstream side of the hull. On the upstream side of the hull, more separation was observed from mid-ship to the stern as a result of high speed flow over the chine at full scale. This was also seen at model scale to a lesser degree. At yaw angles 50 degrees and above the pressure on the downstream side of the hull was noticeably less at full scale than at model scale. As such,

the pressure gradient from the upstream and downstream sides of the hull was greater at full scale which corresponds to the larger lift and drag coefficients at yaw angles greater than 50 degrees.

The escort steering and braking forces of the tug were calculated for both model and full scale cases. The yaw angle at which the maximum steering force was achieved was 40 degrees at model scale and 45 degrees at full scale. The maximum steering force at full scale was found to be 11.6% greater than at model scale. This difference is considered to be due to unequal Reynolds numbers between the two scales as the Froude number was kept constant.

4.4 Future Work

In order to further investigate the physical characteristics of indirect escort operations, the following research should be conducted:

- Carry out additional CFD simulations using various turbulence models at various yaw angles around the stall point to determine the best method for reducing the error associated with force prediction in highly separated flows.
- Include Z-drives in the escort CFD model to compare their influence on hydrodynamic lift and drag forces on the hull and skeg.
- Obtain accurate nozzled Z-drive thrust data for a range of in-flow angles to the nozzle and prop in order to estimate the generated Z-drive forces at a range of yaw and azimuth angles.
- Create an escort CFD model with six degrees-of-freedom that includes the Z-drives and towline in order to eliminate the errors associated with escort force post-processing and to capture the dynamic effects associated with escort operations.

Bibliography

Baniela, Santiago Iglesias. "Roll Motion of a Ship and the Roll Stabilising Effect of Bilge Keels." *The Journal of Navigation*, 2008: 667-686.

Brandner, Paul, and Martin Renilson. "Interaction Between Two Closely Spaced Azimuthing Thrusters." *Journal of Ship Research* 42 (1998): 15-32.

Brooks, Capt. G. V. "Escort Planning." *Towing Solutions Inc.* n.d. http://www.towingsolutionsinc.com/technology-escort_planning.html (accessed 05 10, 2012).

Brooks, Capt. G. V., and V. J. Schisler. "Suggested Tractor Command Language." *Towling Solution Inc.* n.d. http://www.towingsolutionsinc.com/technology-suggested_tractor_command_language.html (accessed May 8, 2012).

CD-adapco. "User Guide STAR-CCM+ Version 6.04.014." 2011.

Froude, W. *Observations and Suggestions on the Subject of Determining by Experiment the Resistance of Ships.* London: The Institution of Naval Architects, 1955.

Harvald, Sven Aage. *Resistance and Propulsion of Ship.* John Wiley & Sons, 1983.

Jukola, Hannu. "Z-Drive Escort Tug Operating Modes." *Marine Technology and SNAME News*, July 1995: 193-196.

Lap, A. J. W. *Resistance (Fundamentals of Ship Resistance and Propulsion).* International Ship Building Progress, 1956.

Molyneux, David, and Neil Bose. "Escort Tug at Large Yaw Angle: Comparison of CFD Predictions with Experimental Data." 2007.

Molyneux, W.D., and G. Earle. *A Comparison of Forces Generated by a Hull and Three Different SKegs for an Escort Tug Design.* Research Report, Fort St. John: National Research Council Canada Institute of Marine Dynamics, 2001.

Morch, Hans Jorgen, Sven Enger, Milovan Peric, and Eberhard Schreck. "Simulation of Lifeboat Launching Under Storm Conditions." *6th International Conference on CFD in Oil & Gas, Metallurgical and Process Industries.* Trondheim, 2008.

Peric, M., D. Jűrgens, M. Palm, and E. Schrek. "Prediction of Resistance of Floating Vessels." *RINA Marine CFD.* Southampton, UK: The Royal Institute of Naval Architects, 2008.

Raven, H.C., A. van der Ploeg, A. R. Starke, and L. Eca. "Towards a CFD-Based Prediction of Ship Performance - Progress in Predicting Full-Scale Resistance and Scale Effects." *RINA Marine CFD.* Southampton, UK: The Royal Institute of Naval Architects, 2008.

Rodi, W. "Experience with Two-Layer Models Combining the k-e Model with a One-Equation Model Near the Wall." *The 29th Aerospace Sciences Meeting.* Reno, NV: AIAA, 1991.

Schlichting, H., and K. Gersten. *Boundary Layer Theory.* New York: Springer, 2000.

Shih, T. H., W. W. Liou, A. Shabbir, Z. Yang, and J Zhu. *A New k-e Eddy Viscosity Model for High Reynolds Number Turbulent Flows -- Model Development and Validation.* NASA TM 106721, 1994.

Versteeg, H K, and W Malalasekera. *An Introduction to Computational Fluid Dynamics.* Harlow: Pearson Education Limited, 1995.

Viola, IM, RG J Flay, and R Ponzini. "CFD Analysis of the Hull Resistance of Small Crafts." *Developments in Marine CFD.* London: RINA, 2011.

White, Frank M. *Fluid Mechanics.* New York: McGraw-Hill, 2003.

Wilcox, David C. *Turbulence Modeling for CFD.* DCW Industries, Inc., 2006.

Appendix A: Mesh Parameters

Table 16: General Meshing Parameters

Parameter	Unit	Full Scale	Model Scale
Base Size	m	5.0	0.5
Number of Prism Layers		7	5
Prism Layer Thickness	m	0.050	0.025
Thickness of Near Wall Prism Layer	mm	0.97	2.17
Default Growth Rate		Slow	Slow
Boundary Growth Rate		Slow	Slow

Table 17: Surface Meshing Parameters

Surface	Relative Minimum Size	Relative Target Size
Deck	1.0%	10.0%
Hull	0.78%	1.6%

Appendix B: Validation Study Results

Table 18: Resistance Validation - Experimental and CFD Results – 1:23.72 Scale

Full Scale Speed	Model Scale Speed	Resistance		
(knots)	(m/s)	Experimental (N)	CFD (N)	Difference (%)
6.0	0.131	1.16	1.18	1.71
8.0	0.174	2.14	2.28	6.33
10.0	0.216	3.96	4.24	6.83
11.0	0.238	5.56	6.08	8.93
12.0	0.259	8.01	8.34	4.04
12.9	0.281	10.1	11.1	9.25
13.9	0.302	12.9	14.1	8.89
14.9	0.323	18.5	18.9	2.36

Table 19: Escort Validation - Experimental and CFD Results at 8 knots – 1:18 Scale

Yaw Angle	Drag Force			Lift Force		
(deg)	Experimental (N)	CFD (N)	Difference (%)	Experimental (N)	CFD (N)	Difference (%)
1.4	20.7	18.9	8.7%	3.8	5.6	-47.5%
11.4	26.9	25.6	4.7%	52.2	46.5	11.0%
16.5	36.2	33.7	7.0%	74.1	69.6	6.0%
21.5	52.0	45.5	12.4%	93.7	91.6	2.2%
26.5	71.7	64.4	10.2%	114.7	109.1	4.9%
31.5	94.5	86.1	8.9%	131.5	129.0	1.9%
36.5	113.0	102.4	9.4%	131.4	131.0	0.3%
41.6	127.7	109.4	14.3%	118.2	99.1	16.2%
46.6	151.1	131.4	13.1%	117.9	84.0	28.7%

Appendix C: Escort Performance

Table 20: 1:10 Model Scale CFD Escort Performance Simulation Results

Run #	Yaw Angle	Heel Angle	Shear Drag	Pressure Drag	Total Drag	Lift	Rolling Moment	Pitching Moment	Yawing Moment	Frontal Area	Wetted Area	Drag Coefficient (10^{-2})		Lift Coefficient (10^{-2})	
	(deg)	(deg)	(N)	(N)	(N)	(N)	(N-m)	(N-m)	(N-m)	(m^2)	(m^2)	Frontal Area	Wetted Area	Frontal Area	Wetted Area
1	0	0.0	-16.9	-12.9	-29.8	0.00	0.00	96.4	0.00	0.490	5.45	-7.06	-0.63	0.00	0.00
2	10	3.4	-17.4	-34.1	-51.5	-129	24.4	97.4	-199	0.603	5.48	-9.83	-1.08	-24.7	-2.72
3	20	6.9	-17.7	-134	-152	-352	54.4	97.7	-413	0.789	-5.55	-22.1	-3.15	-51.3	-7.29
4	30	9.4	-17.2	-346	-363	-625	79.2	88.3	-624	1.01	5.66	-41.3	-7.39	-70.9	-12.7
5	40	9.9	-15.5	-639	-654	-815	71.8	113.5	-781	1.22	5.76	-61.7	-13.1	-76.8	-16.3
6	45	9.5	-11.5	-728	-740	-749	82.0	94.0	-743	1.31	5.73	-65.1	-14.9	-66.0	-15.1
7	50	9.2	-8.49	-599	-608	-215	110	-600	-392	1.35	5.63	-52.1	-12.5	-18.4	-4.40
8	60	7.2	-6.59	-785	-791	-182	44.9	-652	-400	1.48	5.62	-61.8	-16.2	-14.2	-3.74
9	70	6.8	-5.09	-900	-905	-79	32.3	-651	-352	1.61	5.70	-65.0	-18.3	-56.8	-1.60
10	80	5.8	-3.39	-963	-967	28	21.3	-523	-302	1.63	5.62	-68.3	-19.8	1.96	0.568
11	90	4.8	-4.17	-911	-915	128	8.50	-401	-246	1.64	5.61	-64.4	-18.8	10.2	2.98

Table 21: Full Scale CFD Escort Simulation Results

Run #	Yaw Angle	Heel Angle	Shear Drag	Pressure Drag	Total Drag	Lift	Rolling Moment	Pitching Moment	Yawing Moment	Frontal Area	Wetted Area	Drag Coefficient (10^{-2})		Lift Coefficient (10^{-2})	
	(deg)	(deg)	(kN)	(kN)	(kN)	(kN)	(kN-m)	(kN-m)	(kN-m)	(m^2)	(m^2)	Frontal Area	Wetted Area	Frontal Area	Wetted Area
1	0	0.0	-9.94	-9.24	-19.2	0.00	0	976	0	48.5	540	-4.55	-0.409	0.00	0.00
2	10	3.4	-10.2	-30.1	-40.3	-130	230	1,200	-2,030	60.0	543	-7.74	-0.855	-25.0	-2.76
3	20	6.9	-10.3	-134	-144	-376	515	1,790	-4,300	78.5	550	-21.2	-3.02	-55.2	-7.88
4	30	9.4	-9.99	-355	-365	-673	721	2,640	-6,500	101	559	-41.5	-7.52	-76.5	-13.9
5	40	9.9	-8.77	-680	-689	-900	661	4,300	-8,020	123	571	-64.5	-13.9	-84.3	-18.2
6	45	9.5	-7.32	-838	-845	-940	399	1,920	-8,780	132	570	-73.8	-17.1	-82.1	-19.0
7	50	9.2	-4.06	-838	-842	-565	748	5,540	-4,600	137	560	-70.8	-17.3	-47.5	-11.6
8	60	7.2	-3.53	-1,000	-1,000	-284	493	5,310	-2,930	150	562	-76.9	-20.6	-21.8	-5.82
9	70	6.8	-2.61	-1,080	-1,080	-169	115	6,240	-2,670	159	560	-78.7	-22.3	-12.3	-3.47
10	80	5.8	-1.17	-1,100	-1,100	-10.0	-0.54	3,970	-1,910	163	563	-77.5	-22.5	-0.71	-0.21
11	90	4.8	-2.35	-1,080	-1,080	182	-222	7,190	-3,090	165	557	-75.3	-22.3	12.7	3.77